© 2026. Published by The Company of Biologists | Journal of Cell Science (2026) 139, jcs265129. doi:10.1242/jcs.265129

RESEARCH ARTICLE

Antiparallel dimerization of Obscurin controls M-line assembly in *Drosophila* indirect flight muscle

Anja Katzemich[1], Szilárd Szikora[2], Lauren Kowalski[1], Tianrui Wang[1], Péter Bíró[3], Miklós Erdélyi[3], József Mihály[2,4] and Frieder Schöck[1,*]

ABSTRACT

The giant scaffold protein obscurin plays a crucial role in anchoring thick filaments at the muscle M-line. Here, we show that *Drosophila* Obscurin (Obsc) forms an antiparallel dimer at the M-line, with the N-terminal SH3–DH–PH domain facing outwards toward the thin filaments, and the C-terminal kinase region involved in dimerization or oligomerization as well as myosin binding. This arrangement is supported by myosin co-immunoprecipitation, yeast two-hybrid and super-resolution microscopy data, as well as specific Obscurin mutants. Whereas deletion of the N-terminal domains of Obscurin predominantly affects peripheral thin filament length, loss of the C-terminal kinase region of Obscurin disrupts early sarcomere assembly, leading to various defects during sarcomere maturation, supporting its role in keeping thick filaments in register. In conclusion, we propose that Obscurin forms a structural and elastic component organizing thick filaments with its C-terminal kinase region at the M-line, while connecting to thin filaments with its N-terminal domains.

KEY WORDS: Obscurin, M-line, H-zone, *Drosophila*, Indirect flight muscle, Sarcomere assembly

INTRODUCTION

Myofibrils are the contractile structures of striated muscle, composed of serially repeated sarcomeres that generate force through the precise organization of actin and myosin filaments. Within each sarcomere, thin actin filaments are anchored at the Z-discs, whereas thick myosin filaments are crosslinked at the M-line, forming a highly ordered lattice. While actin and myosin constitute the contractile core, sarcomere assembly and stability depend on an extensive network of structural and signaling proteins that organize filament alignment, coordinate mechanical force transmission and maintain myofibril integrity. Among the most prominent of these are giant modular proteins of the titin family, which link multiple sarcomeric regions and contribute to sarcomere stiffness, elasticity and structural organization. Within this family, obscurin proteins have emerged as critical regulators of myofibril assembly and sarcomere integrity (Di Paola and Schöck, 2025).

Obscurins are evolutionarily conserved modular proteins, first identified as UNC-89 in *Caenorhabditis elegans* muscle, where it localizes to the M-line and is required for A-band organization (Benian et al., 1996; Small et al., 2004; Qadota et al., 2008). In vertebrate muscle, the family comprises obscurin (OBSCN), obscurin-like 1 (OBSL1) and the smaller protein called striated muscle preferentially expressed gene (SPEG) (Young et al., 2001; Sutter et al., 2004; Geisler et al., 2007; Fukuzawa et al., 2008; Pernigo et al., 2010; Luo et al., 2021). Obscurins are large multi-domain proteins comprising tandem immunoglobulin (Ig) and fibronectin type III (Fn3) domains, as well as signaling domains, including a src homology 3 (SH3) domain, a Dbl homology (DH) and pleckstrin homology (PH) domain forming a tandem rho-guanine exchange factor (RhoGEF) unit, a Ca^{2+}/calmodulin-binding IQ motif, and two C-terminal kinase domains (Kin1 and Kin2) (Young et al., 2001; Bang et al., 2001; Russell et al., 2002; Fukuzawa et al., 2008). Obscurin and OBSL1 are associated with the M-line but exhibit distinct localization patterns, with OBSL1 localized toward the interior of myofibrils and obscurin enriched at the M-line periphery and, in some contexts, at the Z-disc. Their N-terminal Ig domains interact with titin, myomesin and MyBP-C family proteins, contributing to M-line organization (Kontrogianni-Konstantopoulos et al., 2003; Borisov et al., 2004; Bowman et al., 2007; Fukuzawa et al., 2008; Ackermann et al., 2009). Vertebrate obscurin isoforms additionally contain either ankyrin-binding regions, linking obscurin to the sarcoplasmic reticulum (SR), or tandem kinase domains (Russell et al., 2002; Bagnato et al., 2003; Kontrogianni-Konstantopoulos et al., 2003; Fukuzawa et al., 2005; Cunha and Mohler, 2008). Obscurin loss disrupts SR organization while largely preserving sarcomere structure, whereas combined loss of obscurin and OBSL1 reveals overlapping functions in muscle and SR organization (Kontrogianni-Konstantopoulos et al., 2006; Lange et al., 2009; Blondelle et al., 2019). Obscurin has been proposed to extend transversely across the sarcomere, with its C-terminal region positioned at the M-line and its N-terminal region extending toward the sarcomere periphery (Lange et al., 2009). However, whether this organization applies to the kinase-containing obscurin isoforms and whether their C-terminal kinase domains self-associate remain unclear. Pathogenic variants in obscurin family proteins are also linked to cardiomyopathies, muscular dystrophies and cancers (Ackermann et al., 2009; Marston, 2017; Blondelle et al., 2019; Guardia et al., 2021).

Despite the diverse functions attributed to vertebrate obscurins, their large size and structural complexity have made it challenging to define the contributions of individual domains to sarcomere assembly and maintenance. The indirect flight muscles (IFMs) of *Drosophila melanogaster* provide a powerful system to investigate obscurin function, owing to their highly ordered fibrillar

[1]Department of Biology, McGill University, Montreal, Quebec H3A 1B1, Canada. [2]Institute of Genetics, HUN-REN Biological Research Centre, Szeged 6726, Hungary. [3]Department of Optics and Quantum Electronics, University of Szeged, Szeged 6720, Hungary. [4]Department of Genetics, University of Szeged, Szeged 6726, Hungary.

*Author for correspondence (frieder.schoeck@mcgill.ca)

P.B., 0000-0001-8103-6248; M.E., 0000-0001-5152-0020; J.M., 0000-0003-3399-2424; F.S., 0000-0002-1351-0574

This is an Open Access article distributed under the terms of the Creative Commons Attribution License (https://creativecommons.org/licenses/by/4.0), which permits unrestricted use, distribution and reproduction in any medium provided that the original work is properly attributed.

Handling Editor: Richa Rikhy
Received 17 June 2026; Accepted 12 October 2026

Journal of Cell Science (2026) 139, jcs265129. doi:10.1242/jcs.265129

sarcomeres. Many core sarcomeric proteins are conserved between vertebrates and flies. However, *Drosophila* lacks homologs of myomesin and MyBP-C and possesses only few known M-line proteins, such as Zormin, MASK and Bällchen (Ball) (Burkart et al., 2007; Katzemich et al., 2015). *Drosophila* Obscurin (Obsc) is considerably smaller (~475 kDa) than vertebrate obscurins and multiple isoforms are expressed during development, including in the larval, pupal and adult stages. Major IFM isoforms contain tandem Ig and Fn3 domains together with an N-terminal SH3 and DH–PH domain and two C-terminal kinase domains (Katzemich et al., 2012). Unlike vertebrate obscurins, *D. melanogaster* has only one identified obscurin family member and this is expressed throughout the M-line region. Obscurin is required for M-line formation and proper assembly of thick and thin filaments into the sarcomere, thereby establishing a regular H-zone (Katzemich et al., 2012). Loss of Obscurin causes sarcomere defects, including disrupted M-lines and asymmetric thick and thin filaments with abnormal length and polarity. Furthermore, the two C-terminal kinase domains, Kin1 and Kin2, are predicted pseudokinases that function as scaffolding platforms rather than active enzymes (Katzemich et al., 2015; Zacharchenko et al., 2023). Kin1 binds the active kinase Ball, whereas both kinase domains interact with MASK, a large ankyrin-repeat protein. Depletion of either Ball or MASK produces severe IFM defects similar to those seen upon Obscurin knockdown, including fragmented Z-discs and abnormal M-lines (Katzemich et al., 2015). More recently, the crystal structure of *D. melanogaster* Kin1 revealed a canonical kinase fold lacking key catalytic residues, identifying Kin1 as an inactive pseudokinase with scaffolding properties that might function with Kin2 as a regulatory module (Zacharchenko et al., 2023).

How Obscurin organizes the H-zone and aligns thick filaments during myofibrillogenesis remains poorly understood. Here, we examine how distinct Obscurin domains contribute to H-zone organization and thick filament alignment in *Drosophila* muscle. We show that Obscurin adopts an antiparallel organization within the H-zone, established early during myofibrillogenesis and dependent on C-terminal self-interactions. Furthermore, our data reveal distinct functions of the Obscurin N- and C-termini in regulating H-zone organization, M-line assembly and thick filament alignment.

RESULTS

Anti-Obscurin-DH antibody identifies Obscurin isoforms lacking N-terminal domains

As annotated on FlyBase (CG33519), the *Obsc* gene spans a region of approximately 18 kb and consists of 37 exons (Fig. 1A). It produces at least six different isoforms (*Obsc-RC*, *Obsc-RD*, *Obsc-RE*, *Obsc-RF*, *Obsc-RG* and *Obsc-RH*; where '*R*' denotes transcripts), three of which differ mostly in the 5′ region (*Obsc-RF*, *Obsc-RG* and *Obsc-RH*). The biggest possible isoform is estimated to have a molecular mass of 475 kDa. The predicted domain structure consists of an SH3 domain and DH–PH domain in the N-terminus, followed by 21 Ig domains, two Fn3 domains and two kinase domains at the C-terminus (Fig. 1B). Two antibodies were previously generated: anti-Obscurin-Ig1416 (against Ig domains 14 to 16; Burkart et al., 2007) and anti-Obscurin-Kin1 (against the Kin1 domain; Katzemich et al., 2015).

Using these two antibodies, we characterized and confirmed the dominant Obscurin isoforms present in the *Drosophila* thorax and IFM (Fig. 1C). In thoracic tissue, four major isoform bands of approximately 475 kDa were detected with both anti-Obscurin-Ig1416 and anti-Obscurin-Kin1, two of which are specific to the adult IFM – consistent with our previous observations (Katzemich et al., 2012). To determine whether there are indeed isoforms lacking N-terminal domains as indicated on FlyBase, we raised a novel antibody against the N-terminal DH domain of Obscurin (anti-Obscurin-DH, Fig. 1B). Detection with the anti-Obscurin-DH antibody revealed that only the two largest thoracic isoform bands contain this N-terminal domain. Of these DH-domain-containing bands, only the largest is IFM specific and is therefore the only DH-domain-containing isoform band observed in this tissue. Together, these results indicate that the adult IFM contains isoforms with and without the DH domain and highlight isoform diversity at the 5′ end of the *Obsc* gene, corresponding to isoforms that begin downstream of exon 5 as annotated in FlyBase. Assigning the detected bands to specific annotated isoforms is challenging because their predicted molecular masses differ by only a few kilodaltons, causing them to migrate very closely on SDS-PAGE. The largest band likely represents a composite signal from isoforms PD, PC and PE (where 'P' denotes protein isoforms; these correspond to *Obsc-RD*, *Obsc-RC* and *Obsc-RE*, respectively), which have predicted molecular masses of approximately 475 kDa and 473 kDa. The second-largest band likely corresponds to isoforms PF and PH (corresponding to *Obsc-RF* and *Obsc-RH*), with predicted molecular masses of 446 kDa and 440 kDa, respectively. All of these isoforms include the DH-encoding exons in the 5′ region. The third-largest band is consistent with isoform PG (375 kDa; *Obsc-RG*), which lacks the DH-encoding exons; this is supported by the absence of this band when probed with the DH-specific antibody (Fig. 1C). The identity of the fourth band detected in our western blots remains unresolved. The large genomic locus and the presence of alternative transcription start sites suggests we can generate domain-specific mutants of *Obsc*.

Distinct CRISPR/Cas9-generated Obscurin mutants disrupt isoform expression and cause a flightless phenotype

Previous studies have investigated the role and function of Obscurin in *Drosophila* muscle using RNAi-mediated approaches as well as a P-element-based *Obsc* mutant (Katzemich et al., 2012). To better define the role of Obscurin and its various protein domains in the IFM of *Drosophila*, we generated two distinct CRISPR/Cas9-mediated mutants: Δ1–7, which deletes the first seven exons of the largest Obscurin isoforms, including the initial start site, and Δ30–37, which deletes the final seven exons (exons 30–37) of the gene and therefore the C-terminal kinases (Fig. 1A). Each mutant eliminates the epitope recognized by a specific anti-Obscurin antibody: Δ1–7 removes the anti-Obscurin-DH epitope, and Δ30–37 removes the anti-Obscurin-Kin1 epitope (Fig. 1B).

In the Δ30–37 mutant, truncated versions of all four isoforms were still detected, suggesting that N-terminal domains of Obscurin were still stably translated (Fig. 1D). In the Δ1–7 mutant, the four main isoforms were largely absent, with only one faint band detected with the anti-Obscurin-Kin1 antibody. To further evaluate the possible presence of C-terminal Obscurin domains in Δ1–7 mutants, we looked at pupal stages, when IFM myofibrils develop. At 72 h after puparium formation (APF), a smaller isoform persisted in the Δ1–7 mutant (Fig. 1E). We had therefore generated two domain-specific Obscurin mutations that preserved either the N- or C-terminal domains, respectively. Flies from both mutant lines were incapable of flight from the first day after eclosion (AE), suggesting that the truncation of Obscurin causes a developmental defect during IFM myofibrillogenesis (Fig. 1F). We were able to rescue this phenotype in both mutants by introducing

Journal of Cell Science (2026) 139, jcs265129. doi:10.1242/jcs.265129

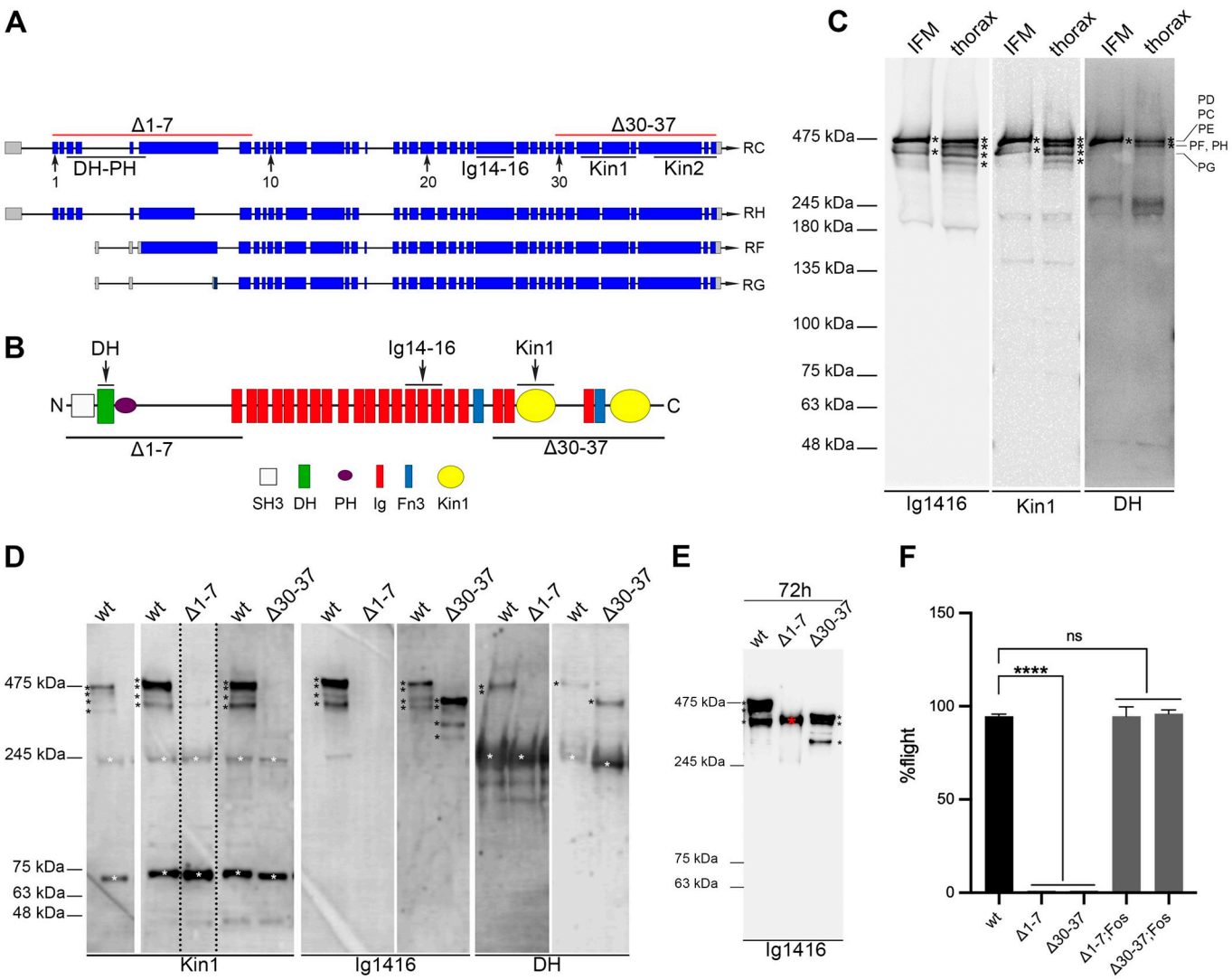

Fig. 1. *Obscurin* CRISPR/Cas9 mutations and their effect on isoforms and flight ability. (A) Schematic representation of *Obscurin* (*Obsc*) transcripts at the *Obsc* locus. The *Obsc* gene consists of 37 exons (blue), represented in the biggest possible transcript, *Obsc-RC* (exons 1, 10, 20 and 30 are indicated). Annotated alternate splice variants, differing in the 5′ end (*Obsc-RF*, *Obsc*-RG and *Obsc-RH*), are shown. We generated two CRISPR/Cas9 mutants (red lines): Δ1–7 and Δ30–37. (B) Predicted protein domains for full-length Obscurin and epitopes of available antibodies (anti-Obscurin-DH, anti-Obscurin-Ig1416 and anti-Obscurin-Kin1) are indicated together with the deletions. (C) Western blots showing Obscurin isoforms in whole thoraces and indirect flight muscles (IFMs). Membranes were incubated with anti-Obscurin-Kin1, anti-Obscurin-Ig1416 and anti-Obscurin-DH. The main isoforms are marked with asterisks. 'P' denotes protein isoforms, corresponding to the respective '*R*' transcript designations in A. *n*=3 independent experiments from different animals. (D) Western blots of thorax samples demonstrating the near-complete loss of all large Obscurin isoforms in Δ1–7 mutant 1-day-old flies compared to their expression in wild-type (wt) flies. A faint band is still visible with the anti-Obscurin-Kin1 antibody. Truncated isoforms are left in the Δ30–37 mutant. Isoforms are indicated by black asterisks. Bands that remain detectable despite deletion of the corresponding antibody epitope, and are therefore considered nonspecific antibody cross-reactions, are indicated by white asterisks. Note that isoforms migrating in close proximity might sometimes not be fully resolved due to the required exposure times. *n*=3 independent experiments from different animals. (E) Western blots of pupal thoraces at 72 h after puparium formation (APF). One isoform is still present in the Δ1–7 mutant (red asterisk). *n*=3 independent experiments from different animals. (F) Flight tests of 1-day-old wild-type and mutant flies. Both mutants lead to a flightless phenotype, which can be fully rescued through the expression of a full-length Obscurin fosmid transgene. *n*=50 animals. Bars show mean±s.d. Statistical significance was assessed using a two-tailed unpaired Student's *t*-test. ns, not significant; ****P<0.0001.

a GFP-tagged full-length Obscurin fosmid (Obsc-Fos; Sarov et al., 2016) into the mutant backgrounds. Obsc-Fos contains most of the regulatory information of Obscurin and expresses it at endogenous levels. Rescue of the flightless phenotypes confirms that they result from the *Obsc* mutations and further supports the functionality of Obsc-Fos, as previously demonstrated (Sarov et al., 2016).

Distinct roles of Obscurin domains in sarcomere integrity

To determine whether these mutants exhibited differential phenotypes, we investigated potential structural abnormalities in their IFMs at 3 days of age using confocal microscopy (Fig. 2A–A″). In wild-type flies, the IFMs exhibited highly organized sarcomeres with precisely aligned Z-discs and M-lines (Fig. 2A). Actin staining revealed consistently well-defined H-zones, visible as dark, straight lines at the center of each sarcomere, reflecting the absence of actin filaments in these regions. Obscurin was labeled with anti-Obscurin-Ig1416 and detected exclusively at the M-line. In the Δ1–7 mutant, H-zones were visible only at the core of the sarcomere, or they were absent altogether (Fig. 2A′). These findings are consistent with our previous RNAi-based observations in which Obscurin

Journal of Cell Science (2026) 139, jcs265129. doi:10.1242/jcs.265129

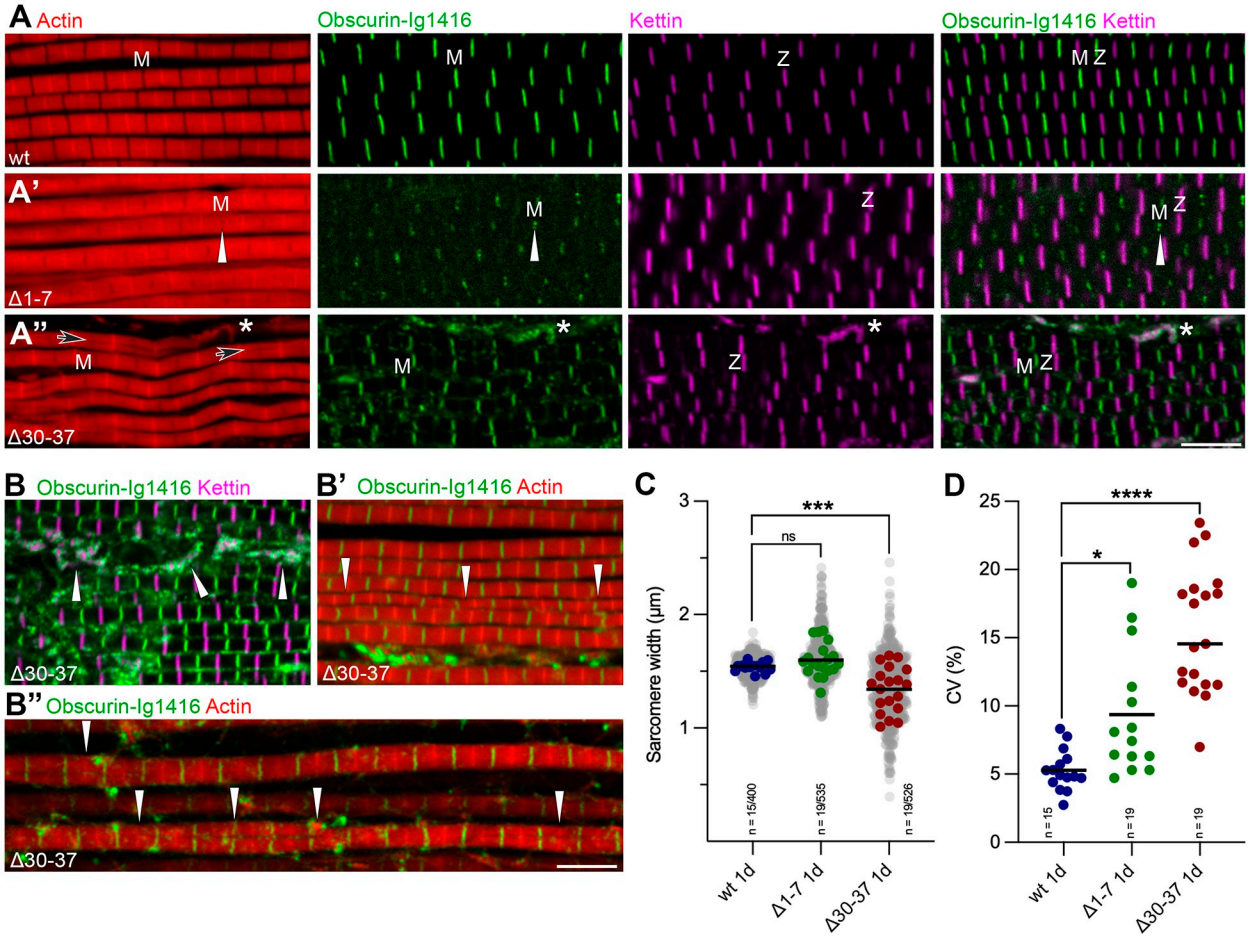

Fig. 2. Effect of Δ1–7 and Δ30–37 mutations on myofibril structure in adult flies. (A–A″) Confocal microscopy images of wild-type (wt, A) and mutant (A′,A″) IFMs labeled with phalloidin (red, actin), anti-Obscurin-Ig1416 (green, M-line, 'M') and anti-Kettin (magenta, Z-disc, 'Z'). (In the Δ1–7 mutant (A′), H-zones are largely absent or restricted to the myofibril core. Obscurin signal is occasionally detected at this site (white arrowheads). In the Δ30–37 mutant (A″), H-zones are also affected, but often visible throughout the width of the sarcomere. Truncated Obscurin isoforms localize to the M-line. Thinned out myofibrils (asterisks) with punctate M-lines and Z-discs are observed. Some myofibrils appear split longitudinally at the sarcomere core (black arrows). Scale bar: 5 µm. (B–B″) Additional prevalent phenotypes in the Δ30–37 mutant (white arrowheads): rudimentary sarcomeres with a dotted appearance (B), reduced myofibril thickness (B′) and myofibrils exhibiting splitting and fusion (B″). Scale bar: 5 µm. (C) Quantification of sarcomere width in 1-day-old wild-type and mutant flies. Solid-color dots represent the mean sarcomere width per animal, calculated from 20–30 myofibrils per animal. Individual measurements are overlaid as semi-transparent grey dots. Bars indicate the mean across animals. *n*-values are shown below each genotype as number of animals/number of individual measurements. (D) Quantification of variability in sarcomere width expressed as the coefficient of variation (CV) for each animal. Statistical significance was assessed by one-way ANOVA followed by Dunnett's multiple comparisons test against the wild type. ns, not significant; **P*<0.05; ****P*<0.001; *****P*<0.0001.

depletion caused pronounced H-zone misalignment and disruption of M-line organization (Katzemich et al., 2012). Despite deletion of the initial start site, the Δ1–7 mutant retained Ig14–16-containing isoforms at the sarcomere core. Although this isoform was not detectable by western blotting in 1-day-old adults (Fig. 1D), its lower abundance relative to the major Obscurin isoforms might preclude detection without overexposing the predominant bands. At 3 days, weak core localization was detected in some IFM regions but was absent in others, consistent with progressive loss of this isoform during IFM maturation. Together with the detection of a smaller isoform at 72 h APF by western blotting (Fig. 1E), these findings support expression of smaller isoforms lacking exons 1–7 from alternative start sites during myofibrillogenesis. In the Δ30–37 mutant, H-zones were often resolved throughout the width of the sarcomere, albeit being less distinct and regular compared to the wild type (Fig. 2A″). Notably, truncated isoforms still localized to the M-line. Often, sarcomeres appeared split longitudinally, originating from the H-zone rather than the Z-disc. In addition, myofibrils frequently showed tapering, with punctate accumulations of Obscurin and Kettin (encoded by *sallimus* or *sls*) at their ends and between adjacent myofibrils. Other prevalent phenotypes included punctate sarcomere-like structures interspersed between mature myofibrils that contained both Obscurin and Kettin (Fig. 2B), as well as visibly thinner myofibrils among those of normal width (Fig. 2B′). In some regions, myofibrils also appeared to undergo cycles of fusion and splitting (Fig. 2B″). Collectively, these structural abnormalities were unique to the Δ30–37 mutant. Unlike RNAi-mediated knockdown, which depleted Obscurin more broadly, both mutants retain distinct Obscurin isoforms, which might account for their differential phenotypes. Both mutants could be fully rescued to wild-type sarcomere structure using Obsc-Fos (Fig. S1).

The frequent appearance of thinner myofibrils in the Δ30–37 mutant prompted us to quantitatively assess sarcomere width and length across genotypes (Fig. 2C; Fig. S2). Quantification of average sarcomere width in 1-day-old flies revealed no significant difference between the wild type and the Δ1–7 mutant, whereas the

Journal of Cell Science (2026) 139, jcs265129. doi:10.1242/jcs.265129

Δ30–37 mutant exhibited a significant reduction in mean sarcomere width. Analysis of individual measurements demonstrates increased variability in both mutants. In the Δ1–7 mutant, sarcomere widths were skewed toward larger values compared to those in the wild type. In contrast, the Δ30–37 mutant displayed substantially greater variability overall, with measurements spanning both smaller and larger values. This increased heterogeneity is further supported by an elevated coefficient of variation calculated per animal, particularly in the Δ30–37 mutant (Fig. 2D). This is consistent with the presence of subpopulations of both thinner and thicker myofibrils in the Δ30–37 mutant. Average sarcomere length was modestly increased in both mutants compared to that in the wild type (Fig. S2A). However, variability in sarcomere length remained largely comparable across genotypes, as reflected by similar coefficients of variation, indicating that alterations in length were relatively uniform and less heterogeneous than those observed for sarcomere width (Fig. S2B).

We also labeled the two mutants with anti-Obscurin-Kin1 and anti-Obscurin-DH antibodies (Fig. S3A,B). Kin1-containing isoforms were weakly present at the remaining M-lines in the core of the myofibril in the Δ1–7 mutant. Δ30–37 lacks the anti-Obscurin-Kin1 epitope; consequently, no signal was detected at the M-line. No DH-containing isoforms could be detected in the Δ1–7 mutant, as it lacks the epitope. In contrast, truncated DH-containing isoforms were observed in the Δ30–37 mutant and localized to the distorted M-line.

To gain a more detailed understanding of the distinct sarcomeric phenotypes, we analyzed both mutants at higher resolution using transmission electron microscopy (Fig. 3). Control sarcomeres showed straight, perfectly centered H-zones spanning the entire width of the myofibrils. Electron-dense spots corresponding to the M-line were clearly visible at the midpoint of the H-zone (Fig. 3A,B). In contrast, in the Δ1–7 mutant, M-lines were disrupted, appearing as fragmented electron-dense aggregates (Fig. 3A′,B′). H-zones were shifted drastically at the periphery of the sarcomere but remained largely in register near the center. Z-discs often did not extend across the entire width of the sarcomeres, with thick and thin filaments bypassing them. In some cases, Z-discs looked broken. Compared to controls, Δ30–37 sarcomeres exhibited H-zones that were also misaligned but typically extended throughout the myofibril (Fig. 3A″,B″). Electron-dense M-line aggregates appeared less pronounced than in Δ1–7 mutants. Remarkably, in Δ30–37 mutants, drastic H-zone shifts were occasionally observed in the sarcomeric core, nearly bisecting the sarcomere along its longitudinal axis in some cases (Fig. 3B″), suggestive of sarcomere splitting. Certain regions of the IFM in this mutant contained sarcomeres resembling two adjacent units fused together (Fig. 3C). Additionally, tapering myofibrils with small Z-discs and poorly defined H-zones were detected, resembling ‘mini-sarcomeres’ that failed to achieve normal width and length, with rudimentary arrangement of thick and thin filaments in between (Fig. 3A″,D). Taken together, these ultrastructural features are consistent with our observations obtained by confocal microscopy.

Overall, deletion of the N-terminal domains (Δ1–7) predominantly compromises peripheral H-zone integrity, whereas loss of the

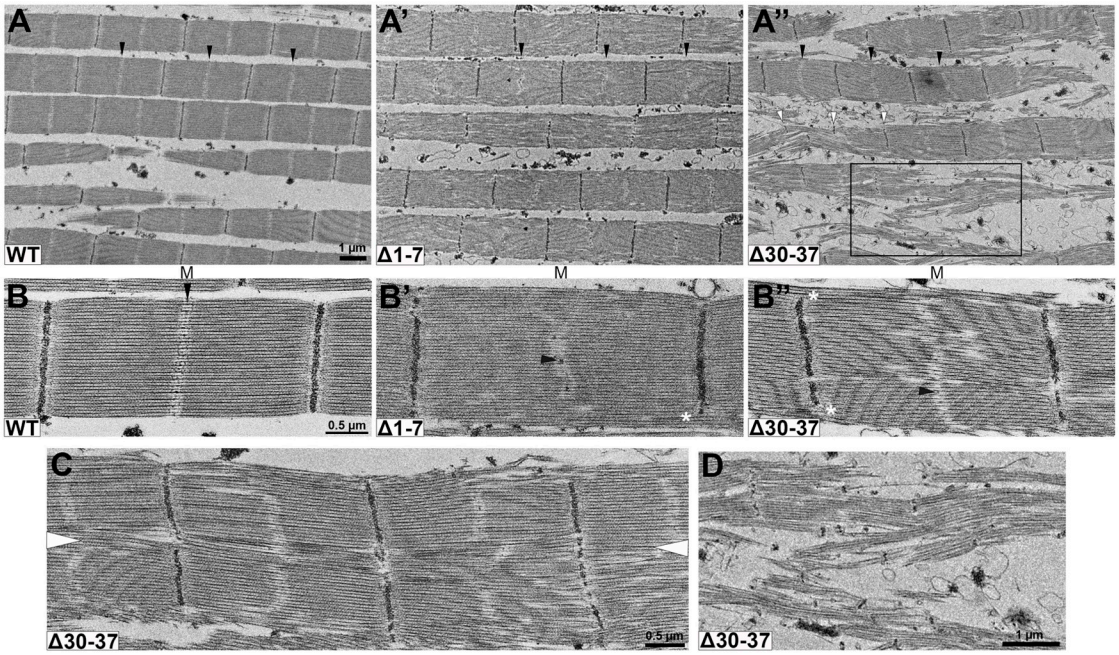

Fig. 3. Distinct H-zone defects revealed by electron microscopy. (A–A″) Compared to the wild-type (WT) IFM (A), in the Δ1–7 mutant IFM (A′), M-lines are disrupted and H-zones are severely shifted at the sarcomere periphery (black arrowheads). The M-line core is often bent but still in the middle of the sarcomere. In the Δ30–37 mutant IFM (A″), M-lines are disrupted and H-zones are wavy but are still centered at the periphery of the sarcomere. Unlike the Δ1–7 mutant, the Δ30–37 mutant also shows small rudimentary sarcomeres with punctate Z-discs (black box, shown at higher magnification in D). Tapering myofibrils with small Z-discs are visible (white arrowheads). Apparent variations in myofibril shape and width in the wild type (A) are due to the angle of sectioning. (B–B″) High-magnification electron micrographs of wild-type and mutant IFMs. In the wild type (B), the M-line appears as a broadening of the thick filament in the middle of the H-zone (black arrowhead). In both mutants (B′,B″), the M-line is disrupted with electron-dense aggregates between thick filaments (black arrowheads). In the Δ1–7 mutant (B′), H-zones are shifted at the periphery, with thick and thin filaments of unequal lengths on either side. In the Δ30–37 mutant (B″), H-zones stay more in register at the periphery but are sometimes out of register or split at the core. In both mutants, Z-discs are often disrupted and do not span the entire width of the sarcomere (white asterisks). (C) High-magnification images of Δ30–37 mutant sarcomeres that appear as two fused myofibrils (white arrowheads). (D) High-magnification view of the black box in A″, highlighting the presence of mini-sarcomeres in the Δ30–37 mutant. Images represent 10 animals.

C-terminal kinase region (Δ30–37) primarily disrupts core sarcomere organization and maturation, highlighting distinct spatial roles of these domains in sarcomere assembly and stability.

Smaller Obscurin isoforms are sufficient for myofibrillar H-zone core formation

As the presence of truncated Obscurin isoforms is clearest during IFM development, we next analyzed the effects of both mutations during pupal development. We immunostained mutant IFMs at different time points during pupal development, namely at 48, 72 and 96 h APF (Fig. 4A). As expected from our observations in adult IFMs, using the anti-Obscurin-Ig1416 antibody, a distinct Obscurin signal was detected at the M-line of the Δ1–7 mutant from 48 h APF onwards. This again confirms that smaller Ig14–16-containing Obscurin isoforms (lacking the N-terminus, including the SH3 and DH–PH domains) are present at the M-line core. At 48 h APF, actin staining revealed that myofibrils in the mutant were less organized than in the wild type, in which H-zones were regularly shaped and well defined. Obscurin localization at the M-line and Kettin incorporation into the Z-disc were also less regular, although an alternate M-line–Z-disc pattern was still maintained. By 72 h APF, myofibrils displayed a more structured appearance with clearly defined H-zones, but Obscurin localization remained somewhat irregular. At 96 h APF, H-zones were markedly affected in the Δ1–7 mutant and the M-line width was narrower than the Z-disc width. In contrast, in the Δ30–37 mutant, Obscurin failed to exhibit a recognizable M-line-labeling pattern at 48 h APF. Instead, it was detected as randomly distributed puncta along the myofibrils, with less sarcomeric regularity than Kettin staining of the Z-discs. By 72 h APF, the Obscurin signal became more organized. At this point, thinner myofibrils as well as split and fused myofibrils could be observed (Fig. 4B). By 96 h APF, Obscurin localized to the distorted M-line and to structures resembling mini-sarcomeres.

To determine whether alterations in sarcomere width arose already during earlier stages of myofibril assembly and thus preceded the phenotype observed in adult flies, we measured sarcomere width at 72 and 96 h APF (Fig. 4C). This analysis revealed a tendency toward reduced myofibrillar width already at 72 h APF, particularly in the Δ30–37 mutant, with distinct populations of significantly thinner myofibrils clearly apparent at this stage (Fig. 4B). By 96 h APF, this reduction became more pronounced and approached the phenotype observed in adult flies. In addition, variability in sarcomere width was significantly increased in the Δ30–37 mutant at 72 h APF and remained elevated at 96 h APF (Fig. 4D). In parallel, we assessed whether sarcomere length undergoes similar developmental changes. Sarcomere length showed a distinct temporal pattern during pupal development (Fig. S4A). In the Δ1–7 mutant, sarcomeres were significantly longer than those in the wild type at both 48 and 72 h APF, but this difference diminished by 96 h APF as values approached wild-type levels. In contrast, the Δ30–37 mutant showed a weaker and less consistent increase in sarcomere length over the same developmental window. However, variability in sarcomere length remained comparable across all genotypes and time points, indicating that the observed differences in length reflect shifts in mean values rather than altered heterogeneity (Fig. S4B).

We also analyzed the same pupal stages of both mutants using the anti-Obscurin-Kin1 antibody (Fig. S5). Similar to the results obtained with anti-Obscurin-Ig1416, we detected Kin1-containing isoforms at the core of the M-line in the Δ1–7 mutant from 48 h APF onwards. At this developmental stage, the less-organized myofibrils resulted in a less regular M-line localization compared to the those in the wild type. Interestingly, at 72 h APF, these isoforms also localized to the Z-disc – an observation not seen in the wild type, in which Kin1-containing isoforms were restricted to the M-line. By 96 h APF, Obscurin-Kin1 was predominantly localized to the M-line in the Δ1–7 mutant. These findings indicate that smaller kinase-containing isoforms with alternative start sites are present at the core and are not affected in the Δ1–7 mutant. In the Δ30–37 mutant, no Kin1 signal was observed at any stage, consistent with the absence of the antibody epitope. This also suggests that mislocalization of Kin1 to the Z-disc in the Δ1–7 mutant is likely real and not due to the ‘stickiness’ of the Z-disc, which sometimes leads to nonspecific labeling.

Finally, we analyzed the two Obscurin mutants using our newly generated DH-specific antibody (Fig. S6). In wild-type IFMs at 48 h APF, we were surprised to detect DH-containing isoforms not only at the M-line, but also at the Z-disc. This provides the first evidence that Obscurin also localizes to the Z-disc in *Drosophila* IFMs. By 72 h APF, DH-containing isoforms were predominantly localized at the M-line, a pattern that persisted at 96 h APF. In the Δ1–7 mutant, which lacks the antibody epitope, we detected a weak anti-Obscurin-DH signal at the Z-disc at 48 h APF, suggesting minor nonspecific antibody staining. However, this signal was considerably weaker than that in the wild type at the same time point. Similar mild nonspecific labeling was also observed at 72 h APF. In the Δ30–37 mutant, Obscurin-DH was initially distributed diffusely across myofibrils, without a distinct localization pattern. By 72 h APF, truncated DH-containing isoforms were localized to the M-line in a somewhat disrupted pattern, and this distribution was maintained at 96 h APF. These findings suggest that C-terminally truncated isoforms are not able to establish a M-line and H-zone during early myofibrillogenesis but are later successfully incorporated into aligned thick filaments (see Discussion).

Antiparallel Obscurin organization is established during early myofibrillogenesis

The essential role of the C-terminal domains of Obscurin in M-line and H-zone assembly suggests that C-terminal domains are involved in keeping thick filaments in register at the center of the M-line. Using super-resolution microscopy, Szikora et al. (2020a) had already proposed that two Obscurin molecules adopt an antiparallel orientation in the H-zone, with their C-termini positioned at the center of the M-line and their N-termini directed toward the thin filaments. This model was inferred from the differential localization of antibodies against the C-terminus (anti-Obscurin-Kin1) and a central region of the protein (anti-Obscurin-Ig1416), which showed that the C-terminal epitope produced a slightly narrower signal. Using our anti-Obscurin-DH antibody, which recognizes the extreme N-terminus, we resolved two distinct lines within the H-zone, separated by an average (±s.d.) distance of 97.9±9.2 nm (Fig. 5A,A′,B,E,E′). This organization directly supports an antiparallel arrangement in which Obscurin N-termini face the pointed ends of thin filaments, whereas central and C-terminal regions localize closer to the M-line (Fig. 5C,D,F).

Having established this antiparallel organization in mature sarcomeres, we next asked when it arises during myofibrillogenesis. To address this, we performed super-resolution imaging of developing IFMs starting from 48 h APF using the same antibodies. Remarkably, the anti-Obscurin-DH antibody already resolved two distinct lines at this early stage, indicating that the antiparallel arrangement of Obscurin is established during initial H-zone formation (Fig. 6A). Notably, the spatial distribution of Obscurin epitopes became progressively more compact along the longitudinal axis of the sarcomere over the course of development, spanning ∼140 nm at 48 h

Journal of Cell Science (2026) 139, jcs265129. doi:10.1242/jcs.265129

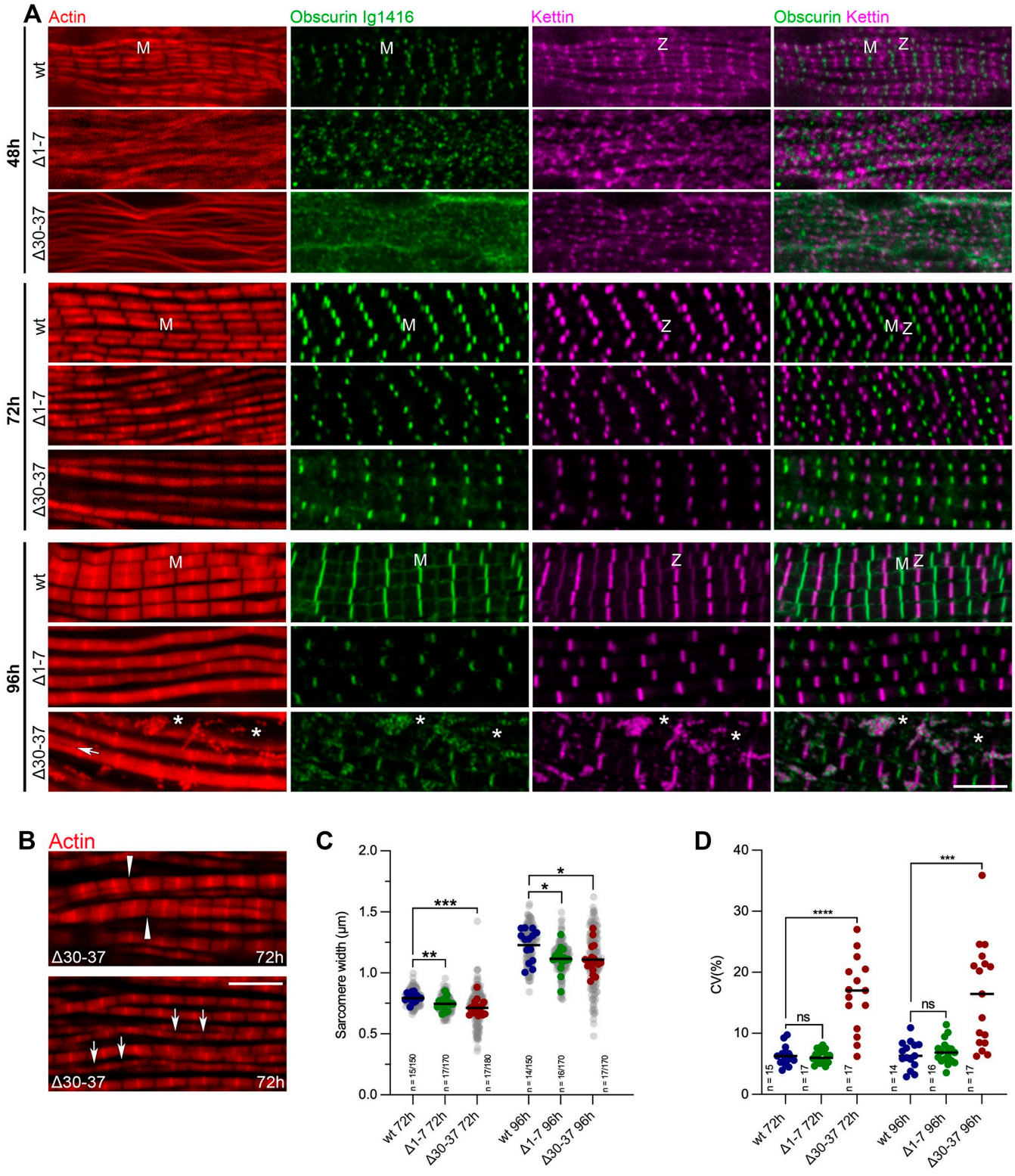

Fig. 4. See next page for legend.

APF and decreasing to ∼100 nm in young adult flies 24 h AE (Fig. 6B,B′). This progressive compaction likely reflects the narrowing of the H-zone during myofibrillogenesis (Görög et al., 2025).

In addition, differential labeling of the M-line by antibodies against the C-terminal kinase domain (Kin1) and central Ig14–16 domains revealed a previously unrecognized spatial organization within the H-zone. Whereas the Kin1 signal extended across the full width of the M-line, including the extreme periphery, Ig14–16 labeling was restricted and excluded from these outer regions (Fig. S7).

Super-resolution microscopy therefore suggests that distinct Obscurin domains occupy spatially defined subregions within the M-line, consistent with an antiparallel arrangement along the longitudinal axis, with C-terminal domains defining the outer periphery of the H-zone.

Journal of Cell Science (2026) 139, jcs265129. doi:10.1242/jcs.265129

Fig. 4. The Δ30–37 mutant has severe defects during early pupal IFM development. (A) Wild-type (wt) and mutant IFMs were labeled with phalloidin (red, actin), anti-Ig1416 (green, M-line, 'M') and anti-Kettin (magenta, Z-disc, 'Z') at 48, 72 and 96 h APF. At 48 h APF, myofibrils looked thinner with no clear H-zones, especially in Δ30–37 mutants. At 72 h APF, myofibrils appeared more organized, with clearly resolved H-zones. At 96 h APF, H-zones were poorly resolved or absent. Smaller Obscurin isoforms were detected at the M-line in the Δ1–7 mutant from 48 h onward and remained confined to the core of the growing myofibril. In the Δ30–37 mutant, Obscurin showed a less clearly defined localization pattern at 48 h. Split M-line cores (arrow) and punctate M-lines and Z-discs (asterisks) were observed at 96 h. Scale bar: 5 µm. See also Figs S3 and S4. (B) Additional images of Δ30–37 mutant IFM at 72 h APF, highlighting split and fused myofibrils (arrowheads) as well as thinner myofibrils (arrows). Scale bar: 5 µm. (C) Quantification of sarcomere width in wild-type and mutant pupae at 72 and 96 h APF. Colored dots denote the mean sarcomere width per animal, based on measurements from ten to 15 myofibrils, with individual data points shown as semi-transparent grey dots. Bars represent the average across animals. *n* indicates the number of animals analyzed with corresponding individual measurements. (D) Variability in sarcomere width is shown as the coefficient of variation (CV) calculated for each animal. Statistical analysis was performed using one-way ANOVA with Dunnett's post hoc test comparing all groups to the wild type. Adjusted *P*-values are indicated. ns, not significant; **P*<0.05; ***P*<0.01; ****P*<0.001; *****P*<0.0001.

C-terminal interactions mediate Obscurin self-association at the H-zone

The spatial arrangement of Obscurin within the H-zone suggests that C-terminal interactions might mediate both Obscurin self-association and its anchoring within the sarcomere. We therefore first asked whether Obscurin forms antiparallel dimers through its C-terminus. To test this hypothesis, we employed a yeast two-hybrid assay (Fig. 7). We first examined whether the full C-terminal region (ObscT, Ig domains 19 and 20 through the extreme C-terminus) could self-associate and compared this with the full N-terminal region (ObscN, very N-terminus to Ig domain 4). Yeast co-transformants expressing the C-terminal constructs exhibited robust growth on selective dropout medium, indicating self-interaction, whereas those expressing the N-terminal constructs did not. Furthermore, ObscN did not interact with ObscT (Fig. 7A,B). We therefore decided to determine which C-terminal domains are essential for this self-interaction. We split the C-terminus into five different fragments. These included: (1) Ig19–20; (2) Kin1, together with its C-terminal regulatory tail (CRD), which is required for proper folding and stability (Zacharchenko et al., 2023); (3) the inter-kinase (IK) region, which contains a helix-rich region (HRR); (4) Ig21–Fn3; and (5) Kin2, expressed without its CRD, as this

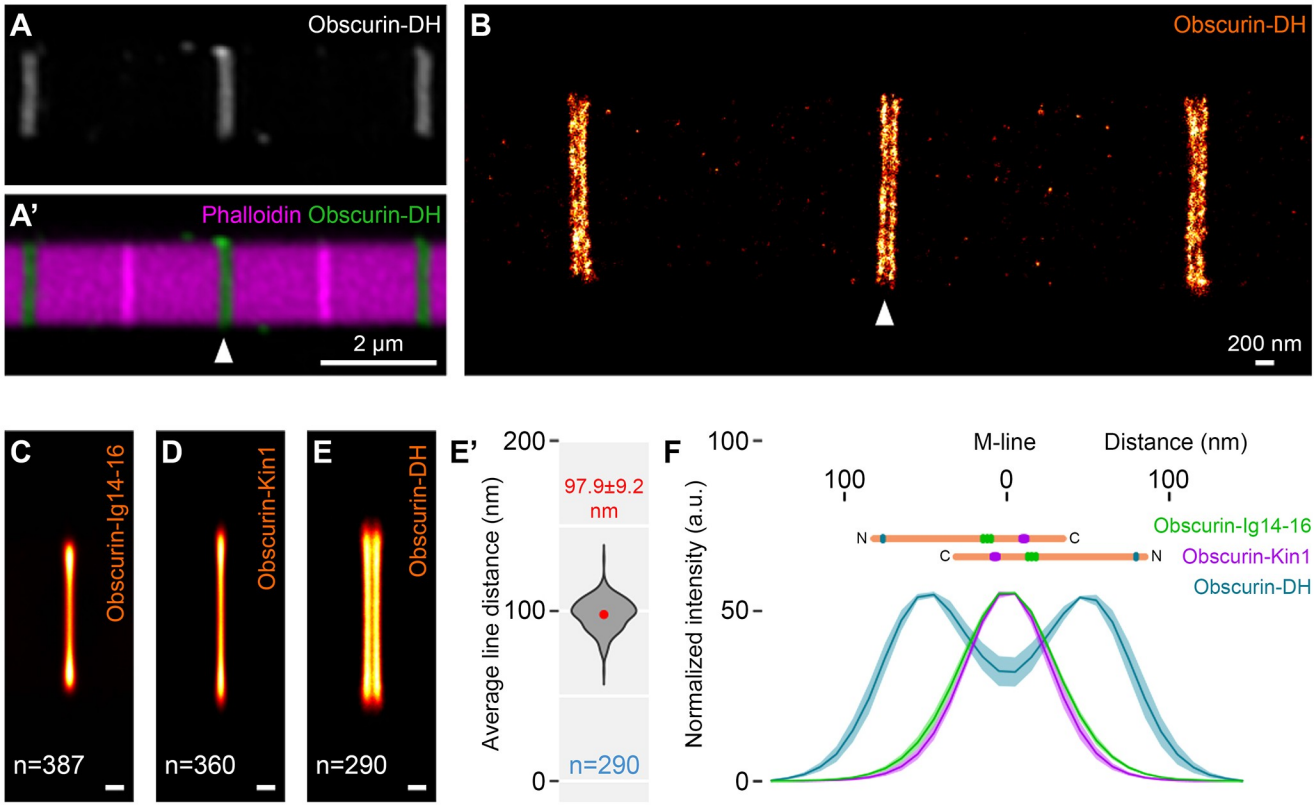

Fig. 5. Nanoscopic localization of Obscurin in the H-zone of mature IFM sarcomeres. (A,A′) Confocal microscopy of isolated individual myofibrils shows that the anti-Obscurin-DH antibody exclusively labels the H-zone (white arrowhead) of mature IFM myofibrils (24 h after eclosion or AE). (B) Direct stochastic optical reconstruction microscopy (dSTORM) image of a myofibril section labeled with the anti-Obscurin-DH antibody reveals two distinct lines within the H-zone. The white arrowhead indicates an H-zone for reference. (C–E) Averaged nanoscopic reconstructions showing the localization of Obscurin Ig14–16, Obscurin Kin1 and Obscurin DH epitopes within the H-zone of mature IFM sarcomeres. *n* indicates the number of sarcomeres used for the averaging. Panel C has been adapted from the data published in Fig. 4F of Görög et al. (2025) under the terms of the CC-BY 4.0 license. Panels D and E represent new experiments. Panels C–E are shown again as the 24 h AE images in Fig. 6A. Scale bars: 200 nm. (E′) Violin plot showing the average distance (red dot) between Obscurin-DH lines (97.9±9.2 nm, indicated as mean±s.d.; *n*=290). (F) Graph depicting the average spatial distribution of Obscurin Ig14–16, Obscurin Kin1 and Obscurin DH epitopes within the H-zone relative to the M-line and to one another. Shaded regions show s.d. a.u., arbitrary units. The schematic illustrates the proposed Obscurin arrangement, in which the N-termini face the pointed ends of thin filaments, whereas the central and C-terminal regions localize closer to the M-line.

Journal of Cell Science (2026) 139, jcs265129. doi:10.1242/jcs.265129

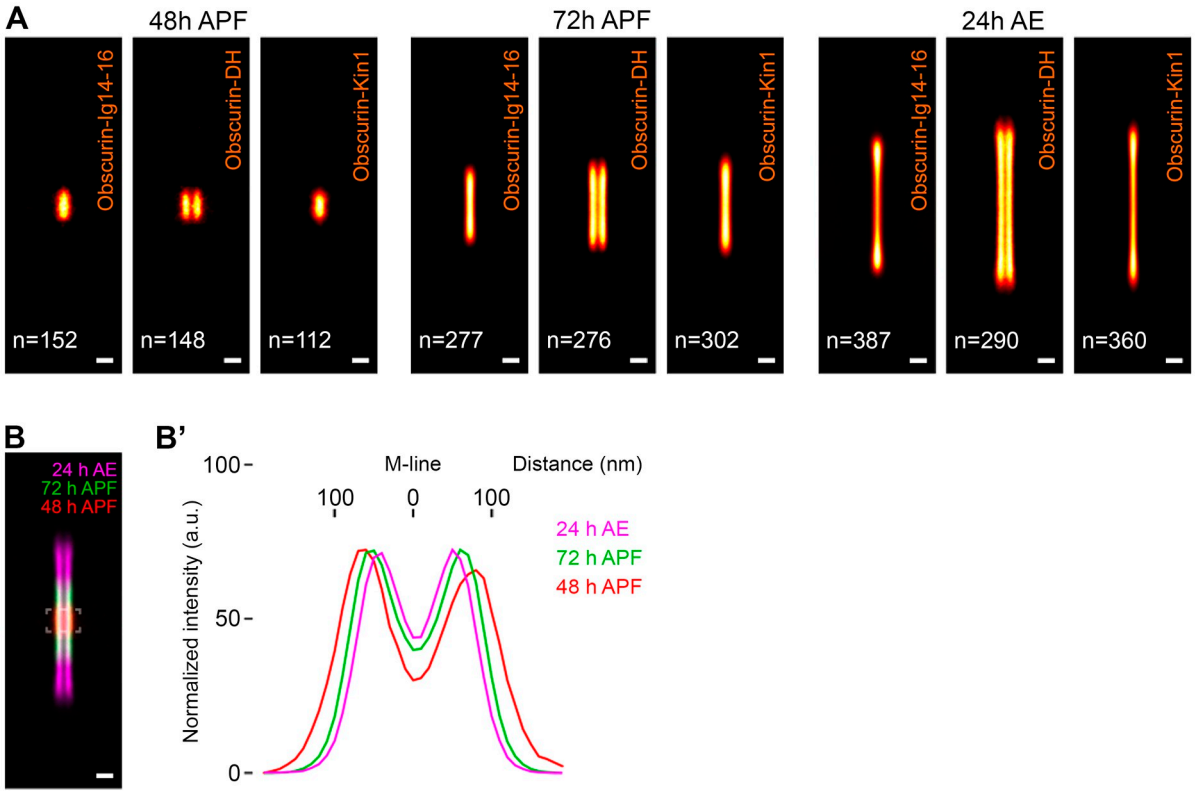

Fig. 6. Nanoscopic localization of Obscurin and the Obscurin-DH epitope within the H-zone during myofibrillogenesis. (A) Averaged dSTORM reconstructions of IFM sarcomeres showing the independent localization of Obscurin Ig14–16, Obscurin DH and Obscurin Kin1 epitopes within the H-zone at 48 h APF, 72 h APF and 24 h AE. *n* indicates the number of sarcomeres included in each average. The Obscurin Ig14–16 sub-panels in A have been adapted from the data published in Fig. 4F of Görög et al. (2025) under the terms of the CC-BY 4.0 license. All other panels represent newly acquired datasets. The 24 h AE images are the same as those shown in Fig. 5C–E. Scale bars: 200 nm. (B) Averaged pseudo-multicolor dSTORM reconstruction comparing Obscurin-DH epitope localization during myofibrillogenesis at 48 h APF (red), 72 h APF (green) and 24 h AE (magenta). The dashed rectangle indicates the region used for intensity profile analysis. Scale bar: 200 nm. (B′) Average intensity profiles of Obscurin-DH epitope distribution across the H-zone relative to the M-line at each developmental stage shown in B.

regulatory tail was reported to interfere with protein–protein interactions (Katzemich et al., 2015). We found that Ig19–20 was capable of strong self-association and also interacted with Ig21–Fn3 as well as ObscT (Fig. 7C). Furthermore, Ig19–20 showed strong growth when co-transformed with the IK domain, which itself showed detectable self-interaction and interacted with ObscT (Fig. 7D). Combinations of other C-terminal domains showed no detectable interactions. We next assessed whether Kin1–CRD could interact with Kin2 (Fig. 7E), based on the previously reported interaction between these two domains (Zacharchenko et al., 2023). Surprisingly, no growth was observed. In contrast, co-transformation of Kin2 with ObscT produced strong growth. We therefore tested an alternative Kin1 construct that extended beyond the CRD to include part of the IK domain. Co-transformation of this longer construct with Kin2 yielded moderate growth, whereas the IK domain alone did not interact with Kin2. Together, these results suggest that regions within the C-terminal portion of Kin1, in combination with a segment of the IK domain, are required for binding to Kin2.

Obscurin C-terminal domains mediate myosin binding

Previous studies have shown that Obscurin interacts with myosin and is essential for anchoring it at the M-line, although it remains unclear whether this interaction is direct and which specific Obscurin domains are involved (Katzemich et al., 2012). The Δ30–37 mutant phenotype and the super-resolution imaging data point to the C-terminal domains mediating myosin binding. To define the mechanisms of Obscurin M-line targeting and myosin binding, we first generated *Obsc* overexpression transgenes dividing the protein into three fragments (Fig. 8A). The N-terminal construct, ObscN, comprises the SH3, DH–PH and Ig1–4 domains; the middle construct, ObscM, includes Ig1–18 and one Fn3 domain; and the C-terminal construct, ObscT, contains the two kinase domains (Kin1 and Kin2), Ig19–21 and a second Fn3 domain. Each construct carries an N-terminal Flag tag and was expressed in a wild-type background using the IFM-specific driver *UH3-GAL4*. ObscN localized to the M-line (Fig. 8B,C). Expression also resulted in pronounced disruption of myofibril organization. In many regions, IFM myofibrils appeared thin and poorly structured, whereas others showed splitting followed by apparent re-fusion. In contrast, ObscM exhibited weak localization to both the M-line and Z-disc and did not disrupt myofibril architecture. Overexpression of the kinase-containing ObscT fragment caused extensive myofibril fusion – a phenotype similar to that observed in the C-terminal Obscurin mutant. ObscT localized strongly to the M-line, with particular accumulation at the M-line periphery and at sites where myofibrils split or fused. Although these results demonstrate that both Obscurin N- and C-terminal domains are sufficient to target the protein to the M-line, the ObscT localization and phenotype were most aligned with super-resolution data and its proposed role in dimerizing at the center of the M-line.

We next evaluated the myosin-binding ability of the Obscurin fragments encoded by these transgenes. To address this, we overexpressed ObscN, ObscM and ObscT in Δ1–7 mutant flies

Journal of Cell Science (2026) 139, jcs265129. doi:10.1242/jcs.265129

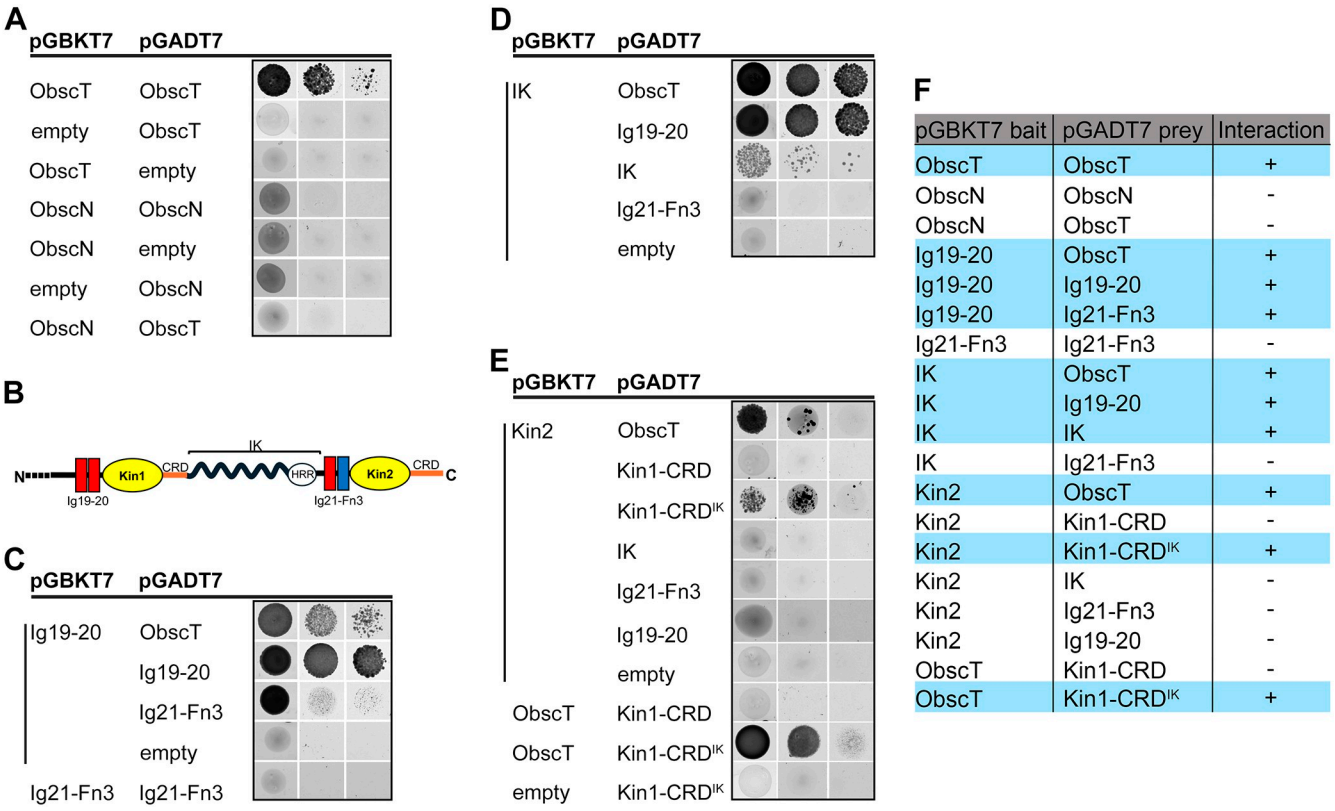

F

pGBKT7 bait	pGADT7 prey	Interaction
ObscT	ObscT	+
ObscN	ObscN	-
ObscN	ObscT	-
Ig19-20	ObscT	+
Ig19-20	Ig19-20	+
Ig19-20	Ig21-Fn3	+
Ig21-Fn3	Ig21-Fn3	-
IK	ObscT	+
IK	Ig19-20	+
IK	IK	+
IK	Ig21-Fn3	-
Kin2	ObscT	+
Kin2	Kin1-CRD	-
Kin2	Kin1-CRD^{IK}	+
Kin2	IK	-
Kin2	Ig21-Fn3	-
Kin2	Ig19-20	-
ObscT	Kin1-CRD	-
ObscT	Kin1-CRD^{IK}	+

Fig. 7. Obscurin forms antiparallel dimers at the H-zone via C-terminal interactions. (A) Yeast two-hybrid (Y2H) co-transformations show that ObscT (Ig19–20–Kin1–Ig21–Fn3–Kin2) self-associates, whereas ObscN (SH3–DH–PH–Ig1–4) does not. *n*=3 independent experiments. (B) Schematic of the Obscurin C-terminus highlighting domain organization (adapted from Zacharchenko et al., 2023). C-terminal regulatory domains (CRDs) following both kinase domains (Kin1 and Kin2) are indicated. The inter-kinase (IK) region contains a helix-rich region (HRR). (C–E) Y2H co-transformations testing interactions between individual domains. Ig19–20 and the IK region exhibit strong self-interaction and also interact with each other. Ig19–20 additionally interacts with Ig21–Fn3. Kin2 interacts only with Kin1–CRD–IK, an extended construct containing part of the IK region. All co-transformations were plated on selective −WLHA medium. Serial dilutions (optical density of 0.1, 0.01 and 0.001) are shown from left to right. *n*=3 independent experiments.
(F) Table summarizing observed Y2H interactions. Positive interactions are highlighted in blue.

using the IFM-specific driver *Act88F-GAL4* and performed immunoprecipitation assays to test which constructs associated with myosin (Fig. 8D). Only ObscT was able to pull down myosin, whereas neither ObscN nor ObscM showed a detectable interaction. Notably, overexpressed ObscT formed additional higher-molecular mass bands even under reducing SDS-PAGE conditions, consistent with dimerization and oligomerization of the Obscurin C-terminus.

DISCUSSION

Muscle contraction requires that thin and thick filaments are in register along the width of the sarcomere. Here, we show how thick filaments are aligned along the M-line in the invertebrate model *Drosophila*, in which Obscurin is the best-characterized M-line scaffold protein to date. Our findings support a model in which Obscurin adopts an antiparallel organization within the H-zone, anchored through C-terminal self-association and positioned to interact directly with myosin via its C-terminal domains, and with the N-terminal regions oriented away from the M-line toward the adjacent thin filaments (Fig. 9). Distinct interaction interfaces within the Obscurin C-terminus, including Ig domains and kinase-associated regions, cooperate to mediate Obscurin–Obscurin and Obscurin–myosin interactions, providing a structural framework for M-line assembly and stabilization during myofibrillogenesis. Although the precise mechanism by which Obscurin crosslinks thick filaments remains unresolved, mutations affecting either the N- or C-terminal regions disrupt M-line assembly and myosin organization, demonstrating that functional cooperation across the length of the molecule is required for proper sarcomere organization and stability.

Antiparallel orientation of Obscurin

An antiparallel orientation of Obscurin within the M-line was first proposed by Szikora et al. (2020a), based on relative localization of epitopes within the middle and C-terminal region of the protein. However, the evidence was limited at the time, because the epitopes of the anti-Obscurin-Ig1416 and the anti-Obscurin-Kin1 antibodies are positioned in proximity within the Obscurin protein. Consequently, the Ig1416 signal resolved only into a wider line relative to that of Kin1 rather than two clearly separated bands, limiting the spatial resolution that could be achieved. The anti-Obscurin-DH antibody against the N-terminus of Obscurin now provides unambiguous evidence for an antiparallel orientation of Obscurin molecules, because the signal resolves into a distinct double line flanking the M-line (Fig. 5). In this model, the C-termini of Obscurin overlap at the center of the M-line, and the N-termini point outward to the thin filaments and H-zone boundaries. This organization is consistent with the proposed role of Obscurin as a molecular scaffold that contributes to thick filament organization and H-zone architecture (Katzemich et al., 2012; 2015; Szikora et al., 2020a). Furthermore, the compaction of the double line from 140 nm

Journal of Cell Science (2026) 139, jcs265129. doi:10.1242/jcs.265129

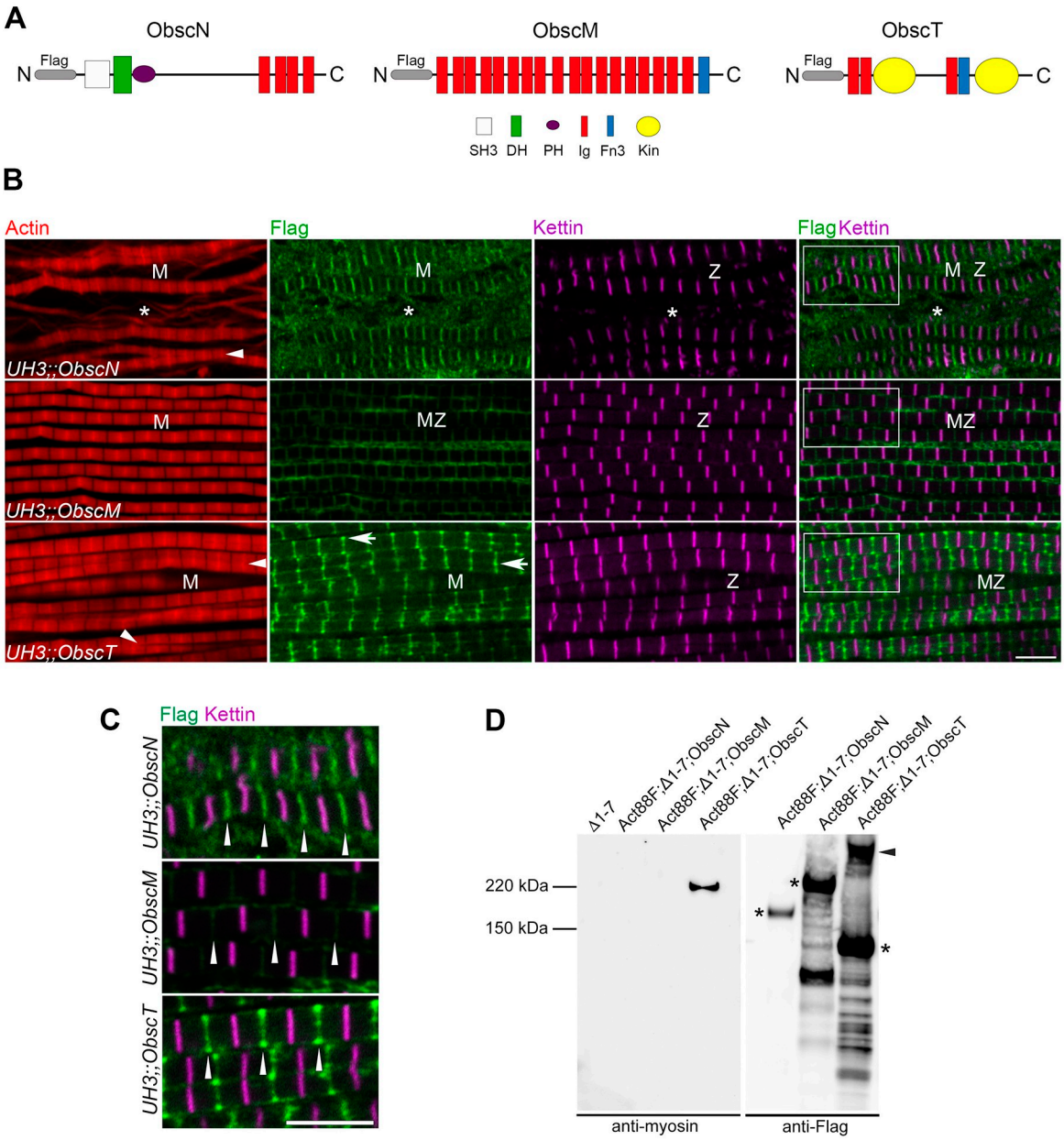

Fig. 8. The Obscurin C-terminal fragment interacts with myosin. (A) Schematic representation of the Flag-tagged Obscurin overexpression fragments: ObscN (SH3–DH–PH–Ig1–4), ObscM (Ig1–18–Fn3) and ObscT (Ig19–20–Kin1–Ig21–Fn3–Kin2). (B) Localization of overexpressed Obscurin fragments in IFMs using the IFM-specific driver *UH3-GAL4* and their effects on myofibrillar organization. IFMs were labeled with phalloidin (red), anti-Kettin (magenta) and anti-Flag (green). ObscN and ObscT localized to the M-line ('M'), whereas ObscM showed weak M-line association and was predominantly distributed between myofibrils. Overexpression of ObscN resulted in thin, rudimentary myofibrils (asterisks), myofibrils that split and re-fused (arrowheads), and shortened sarcomeres that retained a clearly defined H-zone. Overexpression of ObscT led to extensive myofibril splitting and/or fusion (arrowheads), with ObscT accumulating at the sarcomeric periphery and at sites of splitting or fusion (arrows). H-zones remained clearly defined. Overexpression of ObscM did not perturb myofibrillar structure. Z, Z-disc. Images represent 10 animals. Scale bar: 5 µm. (C) Higher-magnification views of the regions outlined by white rectangles in B, highlighting M-line localization of overexpressed fragments (white arrowheads). Scale bar: 5 µm. (D) Co-immunoprecipitation of overexpressed ObscN, ObscM and ObscT with myosin. Only ObscT co-precipitated myosin. Flag-tagged Obscurin fragments were detected using an anti-Flag antibody (asterisks). A higher-molecular-mass ObscT band appeared after incubation (arrowhead), consistent with dimer formation. *n*=3 independent experiments.

to 100 nm during pupal IFM development coincides with the narrowing of the H-zone observed during the same developmental stages (Fig. 6; Görög et al., 2025). It suggests that Obscurin directly contributes to establishing and maintaining H-zone dimensions and spacing during myofibril maturation, rather than serving merely as a passive structural component of the M-line. As Obscurin depletion disrupts thick filament organization and M-line integrity, the observed reduction in spacing could reflect increasing overlap or packing of anti-parallel Obscurin molecules as sarcomeres mature and become more stabilized.

Additional support for the antiparallel arrangement comes from yeast two-hybrid interactions between the C-terminal regions of Obscurin, consistent with a possible self-interaction mechanism (Fig. 7). Our data suggest that an anti-parallel assembly of Obscurin

Journal of Cell Science (2026) 139, jcs265129. doi:10.1242/jcs.265129

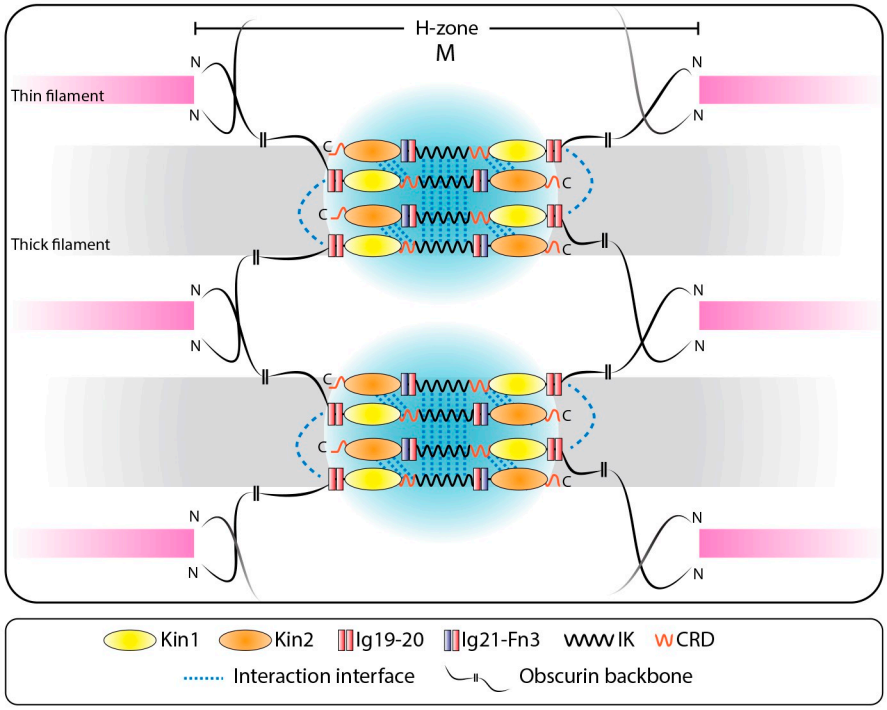

Fig. 9. Proposed model for higher-order Obscurin assembly mediated by multiple C-terminal interaction interfaces. Obscurin functions as a bipolar scaffold within the H-zone of the sarcomere. C-terminal domains localize to the M-line core through interactions with myosin and engage in multiple Obscurin–Obscurin intermolecular interactions (blue dotted lines) that promote Obscurin oligomerization. This generates a higher-order lattice at the M-line core. N-terminal domains localize near the H-zone border where they contribute to H-zone organization through interactions that remain to be determined. For clarity, Obscurin regions outside the indicated domains are represented schematically and are not drawn to scale.

could cluster multiple C-terminal regions at the M-line through interactions involving Ig19–20, Kin1, the IK region and Kin2. Although Kin1 alone did not interact with Kin2, extension of the construct into the IK region enabled binding, indicating that Kin1 and part of the proximal IK region form a functional unit. This interaction aligns with previous findings by Zacharchenko et al. (2023), who also demonstrated that the C-terminal regulatory domain is important for Kin1 folding and stability, while the precise boundary between the Kin1 regulatory region and the IK domain remains unclear. Moreover, structural analysis of Kin1 suggested that it is likely a pseudo-kinase with scaffolding rather than having catalytic properties (Katzemich et al., 2015; Zacharchenko et al., 2023). The localization of kinase domains is a conserved feature of giant sarcomeric proteins, including titin, Projectin (encoded by *bt*) and other Obscurin family proteins, supporting the idea that the M-line functions both as a crosslinking center and a mechanosensitive signaling hub (Kobe et al., 1996; Small et al., 2004; Gautel, 2011). The close proximity of kinase domains within antiparallel Obscurin assemblies might therefore facilitate regulatory interactions either between Obscurin kinase regions or with other M-line-associated kinases such as Ball (Katzemich et al., 2015).

Domain-specific mutations with differential effects on sarcomere integrity

Multiple lines of evidence indicate that our domain-specific mutations of Obscurin provide valuable insight into the distinct functions of its N- and C-terminal regions. First, the anti-Obscurin-DH antibody demonstrates the existence of shorter isoforms without the SH3 and DH–PH domains. These shorter isoforms are also expressed during development. At least one of those isoforms is retained in Δ1–7 mutants, while most isoforms are retained as C-terminal truncations in Δ30–37 mutants (Fig. 1). This observation is confirmed by the weak presence of anti-Obscurin-Ig1416 staining at the M-line core in adult IFM and the stronger staining during pupal development in Δ1–7 mutants. Likewise, the persistence of anti-Obscurin-Ig1416 and anti-Obscurin-DH staining at the M-line in Δ30–37 mutants indicates that C-terminally truncated isoforms retain partial function. Therefore, these mutants selectively disrupt different functional regions of Obscurin and, therefore, provide insight into the respective contributions of N- and C-termini to sarcomere organization and development.

The Δ1–7 phenotype is consistent with the H-zone defects observed following Obscurin RNAi (Katzemich et al., 2012). Importantly, the retention of smaller Obscurin isoforms in the Δ1–7 mutant indicates that these isoforms can support core H-zone organization but are insufficient to maintain H-zone integrity across the full sarcomere width. Δ1–7 mutants can establish the core M-line and H-zone during early myofibril assembly but, as the sarcomere continues to grow in width, it cannot prevent thin filaments from invading the H-zone, resulting in the loss of peripheral H-zones and M-lines (Figs 2–4). These data suggest that the N-terminal SH3 and DH–PH domains contribute to regulate thin filament length or extension, potentially by directly or indirectly interacting with the pointed end of thin filaments. Consistent with this interpretation, Δ1–7 mutants exhibit increased sarcomere lengths during development compared with Δ30–37 mutants (Fig. S4). In vertebrates, DH–PH expression has been reported to increase membrane localization and reduce actin stress fibers, suggesting a link between these domains and actin organization (Shultz et al., 2026). Additionally, altered thick filament symmetry or H-zone positioning could perturb actin–myosin overlap and crossbridge interactions, thereby contributing to asymmetric thin filament extension (Katzemich et al., 2012).

In contrast, Δ30–37 mutants fail to establish H-zones and M-lines in early development (Fig. 4), despite retaining C-terminally truncated Obscurin isoforms. This suggests that these isoforms retain partial function but are insufficient for proper M-line and H-zone organization during early myofibrillogenesis, likely because the self-interaction and myosin-binding domains are missing.

Journal of Cell Science (2026) 139, jcs265129. doi:10.1242/jcs.265129

This leads to a variety of later defects, including mini-sarcomeres lacking characteristic IFM architecture, split and fused myofibrils, and severely out-of-register H-zones and thick filaments (Figs 2–4). Δ30–37 mutants also exhibit smaller mean sarcomere width compared with Δ1–7 mutants, but with strong variability, indicative of a misregulation of sarcomere width (Fig. 4). The appearance of less severely affected sarcomeres can likely be explained by Z-discs being normally established and the titin proteins Kettin and Projectin connecting Z-discs to thick filaments (van Straaten et al., 1999; Bullard et al., 2000; Kulke et al., 2001; Schueder et al., 2023). These interactions might provide a degree of structural constraint on thick filament positioning during development, partially stabilizing sarcomeric organization even in the absence of Obscurin-mediated alignment. However, M-line organization remains consistently perturbed, indicating that Obscurin is required for full and precise register of the thick filament system.

More broadly, these findings also support the idea that giant sarcomeric proteins are expressed as distinct isoforms with specialized spatial and structural roles within the sarcomere. In vertebrates, for example, the homologous proteins obscurin and OBSL1 appear to occupy different regions of the M-line, with obscurin proposed to localize more peripherally and OBSL1 more at the core (Fukuzawa et al., 2008). In *Drosophila*, this is reflected in the differential localization and function of Obscurin isoforms themselves within the M-line and its periphery, as revealed by the Δ1–7 and Δ30–37 phenotypes. Taken together, these data are consistent with a model in which N- and C-terminal Obscurin functions are spatially and temporally segregated during sarcomere assembly, with N-terminal domains contributing to peripheral H-zone alignment, and C-terminal regions supporting stable M-line organization and register. Similarly, proteins such as Sallimus (Sls), Zasp52 and myosin exist as multiple isoforms that localize to distinct positions within the same sarcomeric substructure (Burkart et al., 2007; Orfanos and Sparrow, 2013; González-Morales et al., 2019).

Myosin binding and C-terminal function

Consistent with our genetic and imaging data, overexpression of Obscurin fragments provides further insight into the contribution of the C-terminus in M-line assembly and myosin organization. The C-terminal fragment containing the kinase domains showed distinct M-line localization, with a prominent signal at the periphery of M-lines and at sites of myofibril fusions (Fig. 8B,C), supporting a role of the Obscurin C-terminus in thick filament incorporation and anchoring at the M-line. In contrast, the N-terminal Obscurin fragment showed less distinct M-line localization, although the extent of localization cannot be directly compared between fragments given potential differences in transgene expression levels. The middle region of Obscurin showed no distinct M-line localization, suggesting that stable sarcomeric incorporation requires the N- or C-terminal domains. Importantly, only the Obscurin C-terminus can co-immunoprecipitate myosin, identifying this region as the primary myosin-interacting module of Obscurin (Fig. 8D). In addition, its ability to also form higher-order oligomers, even under denaturing conditions, supports a role of the C-terminus in self-association and is consistent with an antiparallel molecular organization. In agreement with a conserved role of C-terminal Obscurin domains in thick filament organization, deletion of the IK region in *C. elegans* leads to thick filament misalignment, further supporting an evolutionarily conserved role of C-terminal Obscurin domains in sarcomere organization (Qadota et al., 2020).

Together, we propose a model in which Obscurin functions as a bipolar scaffold, with C-terminal domains mediating myosin binding and oligomerization at the M-line core, and N-terminal domains contributing to peripheral H-zone organization, through mechanisms that remain to be determined. The long central region containing tandem Ig and Fn3 domains could provide a flexible connection between these spatially distinct regions. Although the localization of the N-terminal region near the H-zone border raises the possibility of Obscurin binding to proteins in the pointed end area, whether Obscurin interacts with actin or contributes to specification of the position of thin filament ends remains unknown. This spatially segregated architecture could provide a framework for coordinating thick filament alignment and thin filament organization during sarcomere assembly. Rather than forming a single exclusive dimer interface, our yeast two-hybrid data suggest that multiple C-terminal interfaces cooperate to assemble higher-order Obscurin complexes, potentially forming a lattice-like architecture at the M-line. In this framework, Ig19–20 and, likely, the IK domain mediate higher-order multimerization and primary scaffold formation, whereas interactions between a composite Kin1–IK surface and Kin2 promote antiparallel associations between neighboring molecules, thereby stabilizing the complex and contributing to signaling and scaffolding functions (Fig. 9). Together, these interactions could promote staggered or orthogonal lattice-like arrangements that account for the electron-dense M-line structures observed by ultrastructural analysis and might further explain the M-line particles detected by transmission electron microscopy, which are increased in size in the Δ1–7 mutant and reduced in size in the Δ30–37 mutant (Fig. 3). Loss of N-terminal domains enhances Obscurin accumulation at the M-line, consistent with increased self-association and aggregate formation, whereas disruption of C-terminal interaction regions reduces lattice assembly and M-line organization.

Although this model provides a plausible mechanism by which the Obscurin C-terminus contributes to myosin binding, oligomerization and M-line scaffold formation, it remains unclear how Obscurin mediates the crosslinking and precise positioning of neighboring thick filaments within the sarcomere lattice. Importantly, Obscurin localization at the M-line in the Δ30–37 mutant indicates that neither the C-terminal kinases nor Ig19–20 are strictly required for M-line targeting, suggesting that additional interfaces also contribute to intermolecular assembly. Despite not being sufficient for H-zone targeting alone, Ig domains of the central region, in particular around Ig14–16, are potential candidates to serve as additional Obscurin–Obscurin interaction interfaces and could permit the crossed arrangements in our model. Moreover, despite lacking myosin-binding ability, the N-terminal portion of Obscurin is sufficient to provide M-line targeting, indicating that the N-terminal part of Obscurin is able to cooperate with other M-line or H-zone proteins, such as Zormin, or, as suggested by protein localization data, proteins associated with the pointed end of the thin filaments. In the latter case, Obscurin could determine thick filament positioning and, potentially, H-zone width through the combined effects of C-terminal M-line assembly and N-terminal anchorage to the thin filament system. Given the predicted length and flexibility of the central Ig and Fn region, the N-terminal portion is unlikely to function simply as a rigid molecular ruler defining the position of thin filament ends. The central region between the N-terminal domain and Ig19–20/Kin1 contains 20 tandem Ig domains and one Fn domain, corresponding to a minimum estimated length of approximately 84 nm per Obscurin molecule (assuming ∼4 nm per domain). Thus, an antiparallel

arrangement would span approximately 168 nm across the two central regions, substantially greater than the ∼98 nm DH-to-DH distance measured by super-resolution microscopy. This argues against interpreting the central Ig/Fn region as a rigid molecular ruler that directly determines thin filament end position. Alternatively, the broader H-zone observed by direct stochastic optical reconstruction microscopy (dSTORM) analysis (∼133 nm; Szikora et al., 2020a) raises the possibility that the DH epitope lies closer to the M-line rather than marking the exact position of the thin filament ends. Further work is required to determine the precise spatial relationship between Obscurin and the ends of thin filaments, and to better establish the architecture and interaction sites of Obscurin and myosin.

MATERIALS AND METHODS

Fly stocks and genetics

UAS-ObscN (consisting of domains SH3–DH–PH–Ig1–4), *UAS-ObscM* (domains Ig1–18–Fn3) and *UAS-ObscT* (domains Ig19–20–Kin1–Ig21–Fn3–Kin2) transgenic lines were generated by P-element transformation (Genome Prolab). They were crossed to the driver lines *UH3-GAL4* (provided by Upendra Nongthomba, Indian Institute of Science, Bangalore, India) and *Act88F-GAL4* (provided by Richard Cripps, San Diego State University, San Diego, CA, USA; Gajewski and Schulz, 2010). For binding assays in an *Obsc* mutant background, the following stocks were generated and crossed: Δ1–7; *UAS-ObscN*, Δ1–7; *UAS-ObscM*, Δ1–7; *UAS-ObscT*, and *Act88F-GAL4*; Δ1–7. Crosses were incubated at 18°C. For rescue experiments, a GFP-tagged Obscurin fosmid was obtained (fTRG63, Vienna *Drosophila* Resource Center; Sarov et al., 2016) and crossed into the mutant fly background.

Generation of *Obsc* mutants with CRISPR/Cas9

Obsc Δ1–7 was generated by WellGenetics through CRISPR/Cas9-mediated genome editing and homology-dependent repair using two guide RNAs and a double-stranded DNA plasmid donor. The sequences of the two guide RNAs were 5′-TATCGGTTCTACCCAGCAGG[TGG]-3′ and 5′-GCATA-AGCTCCAGGCGGGAT[CGG]-3′, where the bases in brackets are PAM sequences. Exons 1–7 were deleted (∼5 kb). *Obsc* Δ30–37 was generated by GenetiVision using the two guide RNAs 5′-ATATACACCAATACTCA-CTG[AGG]-3′ and 5′-GCAGCTAATTGACTAAAATG[TGG]-3′. Exons 30–37 were deleted (∼4.3 kb).

Molecular procedures and antibody production

All Obscurin expression constructs were synthetized by GenScript and generated by standard cloning procedures. ObscN, ObscM and ObscT with a N-terminal Flag–Strep–His tag were cloned into pUAST (Brand and Perrimon, 1993) for P-element transformation. For yeast two-hybrid assays, the following domains were cloned into the pGBKT7 and pGADT7 vectors (Takara): SH3–DH–PH–Ig1–4 (ObscN), Ig19–20–Kin1–Ig21–Fn3–Kin2 (ObscT), Ig19–20, Kin1–CRD, Kin1–CRD^{IK}, IK, Ig21–Fn3 and Kin2.

For anti-Obscurin-DH antibody production, the DH domain (amino acids 90–263) was amplified from *Drosophila* cDNA via PCR. The fragment was cloned into the expression vector pRSETA (Thermo Fisher Scientific, V35120), which encodes an N-terminal His tag, using standard molecular procedures. The protein was then overexpressed in *Escherichia coli* BL21 and purified under denaturing conditions using a buffer containing 100 mM sodium phosphate, 10 mM Tris-HCl, 8 M urea and 200 mM NaCl (pH 8.0). Rats were immunized following standard procedures (National Research Council Canada, Montreal, Canada).

SDS-page and immunoblotting

Fly thoraces were dissected and homogenized in sample buffer with 6 M urea and protease inhibitors, followed by boiling. Samples were analyzed on 3–8% tris-acetate gradient gels (NuPAGE). The equivalent of 0.5 to 0.25 thoraces was loaded per lane. Gels were immunoblotted and developed using chemiluminescent substrate (BioRad). The primary antibodies used were: rabbit anti-Obscurin-Ig1416 (1:10,000, gift from Belinda Bullard, University of York, York, UK; Burkart et al., 2007), rabbit anti-Obscurin-Kin1 (1:5000, gift from Belinda Bullard; Katzemich et al., 2012) and rat anti-Obscurin-DH (1:5000, this study). Corresponding secondary horseradish peroxidase-conjugated antibodies were used at a dilution of 1:10,000. Uncropped western blots are provided in Fig. S8.

Flight assays

Flight tests were carried out as previously described (Cripps et al., 1994). 1-day-old flies with unfolded wings and hardened cuticles were flight tested. Flies were released inside a Perspex box with a light source on top and scored for the ability to fly up or down.

Immunostainings

For whole-fiber preparations, IFMs were dissected from six to eight glycerinated half thoraces (20 mM sodium phosphate, pH 7.2, 2 mM $MgCl_2$, 2 mM EGTA, 5 mM DTT, 0.5% Triton X-100, 50% glycerol; overnight at −20°C) and washed in relaxing solution (20 mM sodium phosphate, pH 7.2, 5 mM $MgCl_2$, 5 mM ATP, 5 mM EGTA, 5 mM DTT) with protease inhibitors. Samples were fixed for 10 min with 4% paraformaldehyde in relaxing solution. Primary antibody incubation was carried out in relaxing solution overnight at 4°C. This was followed by washes in relaxing solution, and 1–3 h incubations with secondary antibodies. Pupal IFMs were dissected in relaxing solution, fixed in 4% paraformaldehyde in relaxing solution, and labeled with primary and secondary antibodies. Samples were mounted in ProLong Gold antifade solution (Life Technologies, P36930).

Isolation of single myofibrils from the IFM followed the protocol described in Szikora et al., 2020b. In brief, IFM fibers were dissected from glycerinated hemithoraces and mechanically dissociated in an Eppendorf tube with the addition of 0.5% Triton X-100. The resulting myofibrils were centrifuged at 10,000 ***g*** for 2 min at 4°C and resuspended in 200 µl of the relaxing solution described above. This washing and centrifugation procedure was repeated twice. After the final wash, the myofibrils were resuspended in relaxing solution, and 20 µl of the suspension was applied to a glass coverslip and fixed for 20 min with 4% paraformaldehyde. Coverslips were washed three times and blocked in PBS containing 5% goat serum and 0.3% Triton X-100 for 30 min. Primary antibodies were applied in blocking solution and incubated overnight at 4°C. Following additional washes, secondary antibodies were applied for 2 h at room temperature. After thorough washing, samples were mounted in ProLong Gold antifade reagent.

The following primary antibodies were used: rabbit anti-Obscurin-Ig1416 (1:400; gift from Belinda Bullard; Burkart et al., 2007), rabbit anti-Obscurin-Kin1 (1:400; gift from Belinda Bullard; Katzemich et al., 2012), rat anti-Obscurin-DH (1:200, this study), rat anti-Kettin KIg16 (1:400, Developmental Studies Hybridoma Bank, MAC155), rabbit anti-Zasp52 (1:200, Jani and Schöck, 2007), mouse anti-Flag (1:5000, Sigma-Aldrich, F1804). Secondary fluorescently labeled antibodies of the Alexa Fluor series (Life Technologies, Ontario, Canada) were used at 1:500. Rhodamine phalloidin (1:200, Cytoskeleton, Inc., PHDR1) or Alexa Fluor 546-phalloidin (1:200, Life Technologies, P36930) was used to label F-actin. Samples were primarily imaged using confocal microscopy or processed for super-resolution imaging where indicated.

Confocal microscopy

Samples were primarily imaged on a Leica SP8 confocal microscope using a 63×1.4 NA HC Plan Apochromat oil objective. In selected cases, imaging was performed on a Zeiss LSM800 Airyscan system equipped with a Plan-Apochromat 63×/1.40 Oil DIC M27 objective.

Electron microscopy

Half thoraces were glycerinated and processed as described previously (Reedy et al., 1989; Reedy and Beall, 1993; Katzemich et al., 2012). Samples were then washed six times in rigor solution (5 mM MOPS, pH 6.8, 40 mM KCl, 5 mM EGTA, 5 mM $MgCl_2$ and 5 mM NaN_3) and primary fixed in 3% glutaraldehyde and 0.2% tannic acid. This was followed by washes in rigor solution and then 100 mM sodium phosphate, pH 6.0, and 10 mM $MgCl_2$. Secondary fixation was carried out in 1% osmium tetroxide, and samples were subsequently block-stained with 2% uranyl acetate. Samples were dehydrated in an ethanol series,

transferred into epoxypropane and finally embedded with a mix of Embed 812/Araldite (Electron Microscopy Sciences, 13940). Sections were stained with 7% uranyl acetate for 30 min, followed by Sato lead stain (Sato, 1968) for 1 min. Images were acquired on a Tecnai 12 BioTwin 120 kV transmission electron microscope with an AMT XR80C CCD camera (FEI).

Super-resolution dSTORM imaging

Super-resolution imaging was performed as described previously (Szikora et al., 2020a,b). Imaging used a custom-built inverted microscope based on a Nikon Eclipse Ti-E, with a Nikon CFI Apo 100×, NA 1.49 objective. Excitation was provided by a 647 nm laser (MPB Communications, maximum laser power=300 mW), with intensity adjusted to 2–4 kW/cm^2 at the sample via an acousto-optic tunable filter. A 405 nm laser (Nichia, maximum laser power=60 mW) was used for molecule reactivation. Images were collected on an Andor iXon3 897 BV EMCCD camera (512×512 pixels, 16 µm pixel size) as frame stacks. Fluorescence was separated using a Semrock LF405/488/561/635-A-000 filter set with an additional AHF 690/70 H bandpass emission filter. Sample focus was maintained with the perfect focus system (<30 nm precision) of the microscope. Before imaging, the storage buffer was replaced with GLOX switching buffer (Van De Linde et al., 2011), and samples were mounted on microscope slides. Typically, 20,000–50,000 frames were recorded with 20–30 ms exposure.

Image stacks were processed using rainSTORM localization software (Rees et al., 2013), where single-molecule spots were fitted with a Gaussian point-spread function, and their centers were determined. Localization data were filtered for intensity, precision (<20 nm) and standard deviation ($0.8 \leq \sigma \leq 1.0$). Mechanical or thermal drift was corrected using a correlation-based blind drift correction algorithm. Further processing and visualization followed previously described procedures (Szikora et al., 2020a,b; Varga et al., 2023). Briefly, IFM Analyzer v2.1 was used to generate averaged structures by aligning localizations along the H-zone symmetry axis. Super-resolved images were reconstructed at 10 nm pixel size, and pseudo-multicolor images were created by aligning averaged densities along the same symmetry axis. Quantitative analyses were performed either on individual structures to measure line distances or on averages of multiple myofibrils from a single experiment when comparing epitope distributions.

Binding assays

Fifty fly thoraces per genotype (ObscN, ObscM and ObscT, each Flag and His tagged) were bisected in lysis buffer (20 mM Tris-HCl, pH 8.0, 150 mM NaCl, 0.1% Triton X-100, 50% glycerol, complete EDTA-free protease inhibitor cocktail) and left at −20°C overnight. Thoraces were then homogenized in extraction buffer (20 mM Tris-HCl, pH 8.0, 1 M NaCl, 1 mM EDTA, 0.1% Triton X-100, complete EDTA-free protease inhibitor cocktail) and centrifuged for 30 min at 18,300 ***g***. The supernatant was diluted to a final NaCl concentration of 200 mM and incubated with 20 µl prewashed anti-Flag beads (Sigma-Aldrich) for 2 h at 4°C. After incubation and washes with wash buffer (20 mM Tris-HCl, pH 8.0, 200 mM NaCl, 0.1% Triton X-100, complete EDTA-free protease inhibitor cocktail), proteins were eluted with wash buffer containing 200 µg/ml of 3× Flag peptide (Sigma-Aldrich) for 1 h at 4°C. Eluted proteins were then incubated with prewashed Ni-NTA agarose beads (QIAGEN) for 2 h at 4°C. After incubation, beads were washed with wash buffer and bound proteins were eluted by boiling in 2× SDS sample buffer, loaded on a 3–8% acrylamide gel, and transferred onto a nitrocellulose membrane for western blotting. The antibodies used were rat-anti-myosin (Babraham Bioscience Technologies, MAC147) and mouse-anti-Flag antibody (Sigma-Aldrich, F1804) at 1:5000.

Yeast two-hybrid co-transformations

Selected construct pairs, containing defined domains along the Obscurin sequence, were co-transformed into the Matchmaker Y2H Gold strain (Takara) using the lithium-acetate method (Gietz and Schiestl, 2007) and dropped onto selective medium lacking tryptophane and leucine (−WL). Double-transformant colonies were picked and dropped in serial dilutions onto medium lacking tryptophane, leucine, histidine and adenine (−WLHA) to test for protein interactions. Plates were incubated at 30°C.

Image quantification, visualization and statistical analysis

Sarcomere length and width were measured in Fiji using the line tool. Length was defined as the distance between adjacent Z-discs, and width was measured across the Z-disc, with images acquired at the center of the myofibril. For adult IFM sarcomeres, measurements were obtained from 12–19 individual animals, with 20–30 measurements per animal; width variability was assessed by measuring adjacent myofibrils within a 61.57 µm^2 frame, typically containing 25–30 myofibrils. For pupal sarcomeres, measurements were obtained from 13–19 individual animals, with 10–15 measurements per animal. Width variability was similarly assessed by measuring adjacent myofibrils within the same frame. Data were visualized in GraphPad Prism 8 or R. Unless otherwise indicated, data are presented as SuperPlots showing individual measurements overlaid with the mean value for each animal. Statistical analyses were performed using either one-way ANOVA followed by Dunnett's multiple comparisons test (relative to wild type) or a two-tailed unpaired Student's *t*-test.

Acknowledgements

We thank Belinda Bullard, Richard Cripps, Upendra Nongthomba, the Bloomington *Drosophila* Stock Center and the Developmental Studies Hybridoma Bank for materials, FlyBase for access to data, and the Cell Imaging and Analysis network (CIAN) imaging facility at McGill University for access to confocal microscopy. We thank the Facility for Electron Microscopy Research (FEMR) at McGill University for access to and help with electron microscopy.

Competing interests

The authors declare no competing or financial interests.

Author contributions

Conceptualization: A.K., F.S.; Methodology: A.K., S.S., P.B., M.E.; Validation: A.K., S.S.; Formal analysis: A.K., S.S.; Investigation: A.K., S.S., L.K., T.W.; Writing – original draft: A.K., F.S.; Writing – review & editing: A.K., S.S., J.M., F.S.; Visualization: A.K., S.S.; Supervision: J.M., F.S.; Project administration: J.M., F.S.; Funding acquisition: J.M., F.S.

Funding

This work was supported by the Canadian Institutes of Health Research operating grant PJT-178114 to F.S. and by the National Research, Development and Innovation Office of Hungary (Nemzeti Kutatási Fejlesztési és Innovációs Hivatal) through grants K132782 and ADVANCED 153359 to J.M. and FK138894 to S.S. Open Access funding provided by McGill University. Deposited in PMC for immediate release.

Data and resource availability

The authors affirm that all data necessary for confirming the conclusions of this article are present within the article and its supplementary information. All details of resources can be found within the article. Strains and plasmids are available on request.

References

Ackermann, M. A., Hu, L.-Y. R., Bowman, A. L., Bloch, R. J. and Kontrogianni-Konstantopoulos, A. (2009). Obscurin interacts with a novel isoform of MyBP-C slow at the periphery of the sarcomeric M-band and regulates thick filament assembly. *Mol. Biol. Cell* **20**, 2963-2978. doi:10.1091/mbc.e08-12-1251

Bagnato, P., Barone, V., Giacomello, E., Rossi, D. and Sorrentino, V. (2003). Binding of an ankyrin-1 isoform to obscurin suggests a molecular link between the sarcoplasmic reticulum and myofibrils in striated muscles. *J. Cell Biol.* **160**, 245-253. doi:10.1083/jcb.200208109

Bang, M. L., Centner, T., Fornoff, F., Geach, A. J., Gotthardt, M., McNabb, M., Witt, C. C., Labeit, D., Gregorio, C. C., Granzier, H. et al. (2001). The complete gene sequence of titin, expression of an unusual approximately 700-kDa titin isoform, and its interaction with obscurin identify a novel Z-line to I-band linking system. *Circ. Res.* **89**, 1065-1072. doi:10.1161/hh2301.100981

Benian, G. M., Tinley, T. L., Tang, X. and Borodovsky, M. (1996). The Caenorhabditis elegans gene unc-89, required fpr muscle M-line assembly, encodes a giant modular protein composed of Ig and signal transduction domains. *J. Cell Biol.* **132**, 835-848. doi:10.1083/jcb.132.5.835

Blondelle, J., Marrocco, V., Clark, M., Desmond, P., Myers, S., Nguyen, J., Wright, M., Bremner, S., Pierantozzi, E., Ward, S. et al. (2019). Murine obscurin and Obsl1 have functionally redundant roles in sarcolemmal integrity, sarcoplasmic reticulum organization, and muscle metabolism. *Commun. Biol.* **2**, 178. doi:10.1038/s42003-019-0405-7

Borisov, A. B., Kontrogianni-Konstantopoulos, A., Bloch, R. J., Westfall, M. V. and Russell, M. W. (2004). Dynamics of obscurin localization during differentiation

and remodeling of cardiac myocytes: obscurin as an integrator of myofibrillar structure. *J. Histochem. Cytochem. Off. J. Histochem. Soc.* **52**, 1117-1127. doi:10.1369/jhc.3A6183.2004

Bowman, A. L., Kontrogianni-Konstantopoulos, A., Hirsch, S. S., Geisler, S. B., Gonzalez-Serratos, H., Russell, M. W. and Bloch, R. J. (2007). Different obscurin isoforms localize to distinct sites at sarcomeres. *FEBS Lett.* **581**, 1549-1554. doi:10.1016/j.febslet.2007.03.011

Brand, A. H. and Perrimon, N. (1993). Targeted gene expression as a means of altering cell fates and generating dominant phenotypes. *Development* **118**, 401-415. doi:10.1242/dev.118.2.401

Bullard, B., Goulding, D., Ferguson, C. and Leonard, K. (2000). Links in the chain: the contribution of kettin to the elasticity of insect muscles. *Adv. Exp. Med. Biol.* **481**, 207-218; discussion 219-220. doi:10.1007/978-1-4615-4267-4_12

Burkart, C., Qiu, F., Brendel, S., Benes, V., Hååg, P., Labeit, S., Leonard, K. and Bullard, B. (2007). Modular proteins from the Drosophila sallimus (sls) gene and their expression in muscles with different extensibility. *J. Mol. Biol.* **367**, 953-969. doi:10.1016/j.jmb.2007.01.059

Cripps, R. M., Ball, E., Stark, M., Lawn, A. and Sparrow, J. C. (1994). Recovery of dominant, autosomal flightless mutants of Drosophila melanogaster and identification of a new gene required for normal muscle structure and function. *Genetics* **137**, 151-164. doi:10.1093/genetics/137.1.151

Cunha, S. R. and Mohler, P. J. (2008). Obscurin targets ankyrin-B and protein phosphatase 2A to the cardiac M-line. *J. Biol. Chem.* **283**, 31968-31980. doi:10.1074/jbc.M806050200

Di Paola, J. N. and Schöck, F. (2025). The varied functions of the giant muscle scaffold protein obscurin. *Front. Cell Dev. Biol.* **13**, 1689326. doi:10.3389/fcell.2025.1689326

Fukuzawa, A., Idowu, S. and Gautel, M. (2005). Complete human gene structure of obscurin: implications for isoform generation by differential splicing. *J. Muscle Res. Cell Motil.* **26**, 427-434. doi:10.1007/s10974-005-9025-6

Fukuzawa, A., Lange, S., Holt, M., Vihola, A., Carmignac, V., Ferreiro, A., Udd, B. and Gautel, M. (2008). Interactions with titin and myomesin target obscurin and obscurin-like 1 to the M-band – implications for hereditary myopathies. *J. Cell Sci.* **121**, 1841-1851. doi:10.1242/jcs.028019

Gajewski, K. M. and Schulz, R. A. (2010). CF2 represses Actin 88F gene expression and maintains filament balance during indirect flight muscle development in Drosophila. *PLoS ONE* **5**, e10713. doi:10.1371/journal.pone.0010713

Gautel, M. (2011). Cytoskeletal protein kinases: titin and its relations in mechanosensing. *Pflüg. Arch. Eur. J. Physiol.* **462**, 119-134. doi:10.1007/s00424-011-0946-1

Geisler, S. B., Robinson, D., Hauringa, M., Raeker, M. O., Borisov, A. B., Westfall, M. V. and Russell, M. W. (2007). Obscurin-like 1, OBSL1, is a novel cytoskeletal protein related to obscurin. *Genomics* **89**, 521-531. doi:10.1016/j.ygeno.2006.12.004

Gietz, R. D. and Schiestl, R. H. (2007). High-efficiency yeast transformation using the LiAc/SS carrier DNA/PEG method. *Nat. Protoc.* **2**, 31-34. doi:10.1038/nprot.2007.13

González-Morales, N., Xiao, Y. S., Schilling, M. A., Marescal, O., Liao, K. A. and Schöck, F. (2019). Myofibril diameter is set by a finely tuned mechanism of protein oligomerization in Drosophila. *eLife* **8**, e50496. doi:10.7554/eLife.50496

Görög, P., Novák, T., Polgár, T. F., Bíró, P., Gutheil, A., Kozma, C., Gajdos, T., Tóth, K., Tóth, A., Erdélyi, M. et al. (2025). Developmental remodelling of *Drosophila* flight muscle sarcomeres: a scaled myofilament lattice model based on multiscale morphometrics. *Open Biol.* **15**, 250182. doi:10.1098/rsob.250182

Guardia, T., Eason, M. and Kontrogianni-Konstantopoulos, A. (2021). Obscurin: A multitasking giant in the fight against cancer. *Biochim. Biophys. Acta Rev. Cancer* **1876**, 188567. doi:10.1016/j.bbcan.2021.188567

Jani, K. and Schöck, F. (2007). Zasp is required for the assembly of functional integrin adhesion sites. *J. Cell Biol.* **179**, 1583-1597. doi:10.1083/jcb.200707045

Katzemich, A., Kreisköther, N., Alexandrovich, A., Elliott, C., Schöck, F., Leonard, K., Sparrow, J. and Bullard, B. (2012). The function of the M-line protein, obscurin, in controlling the symmetry of the sarcomere in *Drosophila* flight muscle. *J. Cell Sci.* **125**, 3367-3379. doi:10.1242/jcs.097345

Katzemich, A., West, R. J. H., Fukuzawa, A., Sweeney, S. T., Gautel, M., Sparrow, J. and Bullard, B. (2015). Binding partners of the kinase domains in Drosophila obscurin and their effect on the structure of the flight muscle. *J. Cell Sci.* **128**, 3386-3397. doi:10.1242/jcs.170639

Kobe, B., Heierhorst, J., Feil, S. C., Parker, M. W., Benian, G. M., Weiss, K. R. and Kemp, B. E. (1996). Giant protein kinases: domain interactions and structural basis of autoregulation. *EMBO J.* **15**, 6810-6821. doi:10.1002/j.1460-2075.1996.tb01072.x

Kontrogianni-Konstantopoulos, A., Jones, E. M., Van Rossum, D. B. and Bloch, R. J. (2003). Obscurin is a ligand for small ankyrin 1 in skeletal muscle. *Mol. Biol. Cell* **14**, 1138-1148. doi:10.1091/mbc.e02-07-0411

Kontrogianni-Konstantopoulos, A., Catino, D. H., Strong, J. C., Sutter, S., Borisov, A. B., Pumplin, D. W., Russell, M. W. and Bloch, R. J. (2006). Obscurin modulates the assembly and organization of sarcomeres and the sarcoplasmic reticulum. *FASEB J. Off. Publ. Fed. Am. Soc. Exp. Biol.* **20**, 2102-2111. doi:10.1096/fj.06-5761com

Kulke, M., Neagoe, C., Kolmerer, B., Minajeva, A., Hinssen, H., Bullard, B. and Linke, W. A. (2001). Kettin, a major source of myofibrillar stiffness in *Drosophila* indirect flight muscle. *J. Cell Biol.* **154**, 1045-1058. doi:10.1083/jcb.200104016

Lange, S., Ouyang, K., Meyer, G., Cui, L., Cheng, H., Lieber, R. L. and Chen, J. (2009). Obscurin determines the architecture of the longitudinal sarcoplasmic reticulum. *J. Cell Sci.* **122**, 2640-2650. doi:10.1242/jcs.046193

Luo, S., Rosen, S. M., Li, Q. and Agrawal, P. B. (2021). Striated preferentially expressed protein kinase (SPEG) in muscle development, function, and disease. *Int. J. Mol. Sci.* **22**, 5732. doi:10.3390/ijms22115732

Marston, S. (2017). Obscurin variants and inherited cardiomyopathies. *Biophys. Rev.* **9**, 239-243. doi:10.1007/s12551-017-0264-8

Orfanos, Z. and Sparrow, J. C. (2013). Myosin isoform switching during assembly of the Drosophila flight muscle thick filament lattice. *J. Cell Sci.* **126**, 139-148. doi:10.1242/jcs.110361

Pernigo, S., Fukuzawa, A., Bertz, M., Holt, M., Rief, M., Steiner, R. A. and Gautel, M. (2010). Structural insight into M-band assembly and mechanics from the titin-obscurin-like-1 complex. *Proc. Natl. Acad. Sci. USA* **107**, 2908-2913. doi:10.1073/pnas.0913736107

Qadota, H., McGaha, L. A., Mercer, K. B., Stark, T. J., Ferrara, T. M. and Benian, G. M. (2008). A novel protein phosphatase is a binding partner for the protein kinase domains of UNC-89 (Obscurin) in Caenorhabditis elegans. *Mol. Biol. Cell* **19**, 2424-2432. doi:10.1091/mbc.e08-01-0053

Qadota, H., Moody, J. C., Lesanpezeshki, L., Moncrief, T., Kitzler, D., Bhat, P. D., Vanapalli, S. A., Oberhauser, A. F. and Benian, G. M. (2020). A region of UNC-89 (Obscurin) lying between two protein kinase domains is a highly elastic spring required for proper sarcomere organization. *J. Mol. Biol.* **432**, 4799-4814. doi:10.1016/j.jmb.2020.06.024

Reedy, M. C. and Beall, C. (1993). Ultrastructure of developing flight muscle in Drosophila. II. Formation of the myotendon junction. *Dev. Biol.* **160**, 466-479. doi:10.1006/dbio.1993.1321

Reedy, M. C., Beall, C. and Fyrberg, E. (1989). Formation of reverse rigor chevrons by myosin heads. *Nature* **339**, 481-483. doi:10.1038/339481a0

Rees, E. J., Erdelyi, M., Schierle, G. S. K., Knight, A. and Kaminski, C. F. (2013). Elements of image processing in localization microscopy. *J. Opt.* **15**, 094012. doi:10.1088/2040-8978/15/9/094012

Russell, M. W., Raeker, M. O., Korytkowski, K. A. and Sonneman, K. J. (2002). Identification, tissue expression and chromosomal localization of human Obscurin-MLCK, a member of the titin and Dbl families of myosin light chain kinases. *Gene* **282**, 237-246. doi:10.1016/s0378-1119(01)00795-8

Sarov, M., Barz, C., Jambor, H., Hein, M. Y., Schmied, C., Suchold, D., Stender, B., Janosch, S., Vinay Vikas, K. J., Krishnan, R. T. et al. (2016). A genome-wide resource for the analysis of protein localisation in Drosophila. *eLife* **5**, e12068. doi:10.7554/eLife.12068

Sato, T. (1968). A modified method for lead staining of thin sections. *J. Electron Microsc.* **17**, 158-159

Schueder, F., Mangeol, P., Chan, E. H., Rees, R., Schünemann, J., Jungmann, R., Görlich, D. and Schnorrer, F. (2023). Nanobodies combined with DNA-PAINT super-resolution reveal a staggered titin nanoarchitecture in flight muscles. *eLife* **12**, e79344. doi:10.7554/eLife.79344

Shultz, K. D., Ouderkirk, S. N., Al Anbari, Y. F., White, C. J., Henry, P., Kubow, K. E., Conway, D. E., Miller, C. J. and Wright, N. T. (2026). Obscurin a localizes near the cell membrane to modulate stress fiber dynamics and cell migration. *J. Biol. Chem.* **302**, 111383. doi:10.1016/j.jbc.2026.111383

Small, T. M., Gernert, K. M., Flaherty, D. B., Mercer, K. B., Borodovsky, M. and Benian, G. M. (2004). Three new isoforms of caenorhabditis elegans UNC-89 containing MLCK-like protein kinase domains. *J. Mol. Biol.* **342**, 91-108. doi:10.1016/j.jmb.2004.07.006

Sutter, S. B., Raeker, M. O., Borisov, A. B. and Russell, M. W. (2004). Orthologous relationship of obscurin and Unc-89: phylogeny of a novel family of tandem myosin light chain kinases. *Dev. Genes Evol.* **214**, 352-359. doi:10.1007/s00427-004-0413-5

Szikora, S., Gajdos, T., Novák, T., Farkas, D., Földi, I., Lenart, P., Erdélyi, M. and Mihály, J. (2020a). Nanoscopy reveals the layered organization of the sarcomeric H-zone and I-band complexes. *J. Cell Biol.* **219**, e201907026. doi:10.1083/jcb.201907026

Szikora, S., Novák, T., Gajdos, T., Erdélyi, M. and Mihály, J. (2020b). Superresolution Microscopy of Drosophila Indirect Flight Muscle Sarcomeres. *Bio-Protoc.* **10**, e3654. doi:10.21769/BioProtoc.3654

Van De Linde, S., Löschberger, A., Klein, T., Heidbreder, M., Wolter, S., Heilemann, M. and Sauer, M. (2011). Direct stochastic optical reconstruction microscopy with standard fluorescent probes. *Nat. Protoc.* **6**, 991-1009. doi:10.1038/nprot.2011.336

van Straaten, M., Goulding, D., Kolmerer, B., Labeit, S., Clayton, J., Leonard, K. and Bullard, B. (1999). Association of kettin with actin in the Z-disc of insect flight muscle. *J. Mol. Biol.* **285**, 1549-1562. doi:10.1006/jmbi.1998.2386

Varga, D., Szikora, S., Novák, T., Pap, G., Lékó, G., Mihály, J. and Erdélyi, M. (2023). Machine learning framework to segment sarcomeric structures in SMLM data. *Sci. Rep.* **13**, 1582. doi:10.1038/s41598-023-28539-7

Young, P., Ehler, E. and Gautel, M. (2001). Obscurin, a giant sarcomeric Rho guanine nucleotide exchange factor protein involved in sarcomere assembly. *J. Cell Biol.* **154**, 123-136. doi:10.1083/jcb.200102110

Zacharchenko, T., Dorendorf, T., Locker, N., Van Dijk, E., Katzemich, A., Diederichs, K., Bullard, B. and Mayans, O. (2023). PK1 from Drosophila obscurin is an inactive pseudokinase with scaffolding properties. *Open. Biol.* **13**, 220350. doi:10.1098/rsob.220350

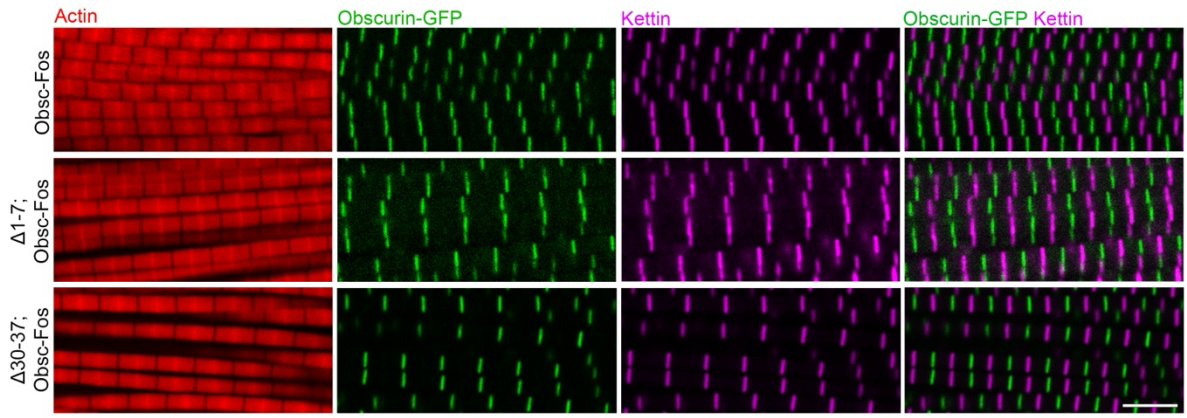

Fig. S1. Rescue of myofibrillar defects in *Obscurin* mutants using a full-length obscurin-GFP fosmid transgene. IFMs were labelled with phalloidin (actin, red) and anti-kettin antibody (magenta). Obscurin-GFP is shown in green. All mutant phenotypes are fully rescued. Scale bar = 5 μm.

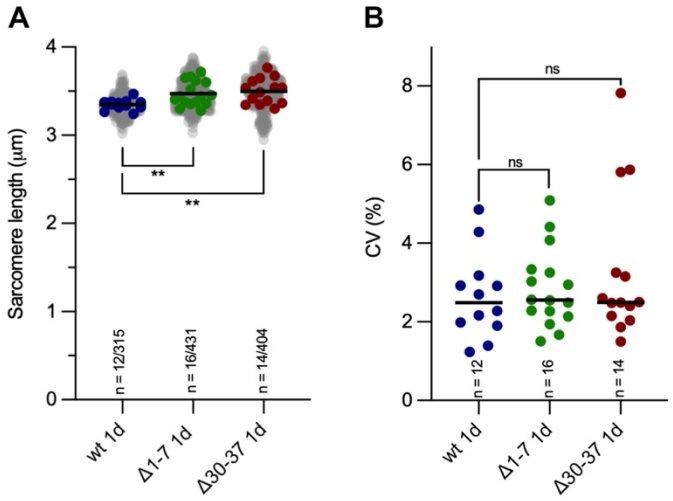

Fig. S2. Analysis of sarcomere length in 1 d-old wild type and mutant flies. (A) Quantification of sarcomere length. Solid-colored dots represent the mean sarcomere length per animal, calculated from 20–30 myofibrils per individual. Individual measurements are shown as semi-transparent grey dots. Bars indicate the mean across animals. *n* values are shown below each genotype as *n* = number of animals/number of individual measurements. (B) Variability in sarcomere length expressed as the coefficient of variation (CV) per animal. Statistical significance was determined by one-way ANOVA followed by Dunnett's multiple comparisons test against wild type. Statistical significance is indicated. ns (not significant); ** $P < 0.001$.

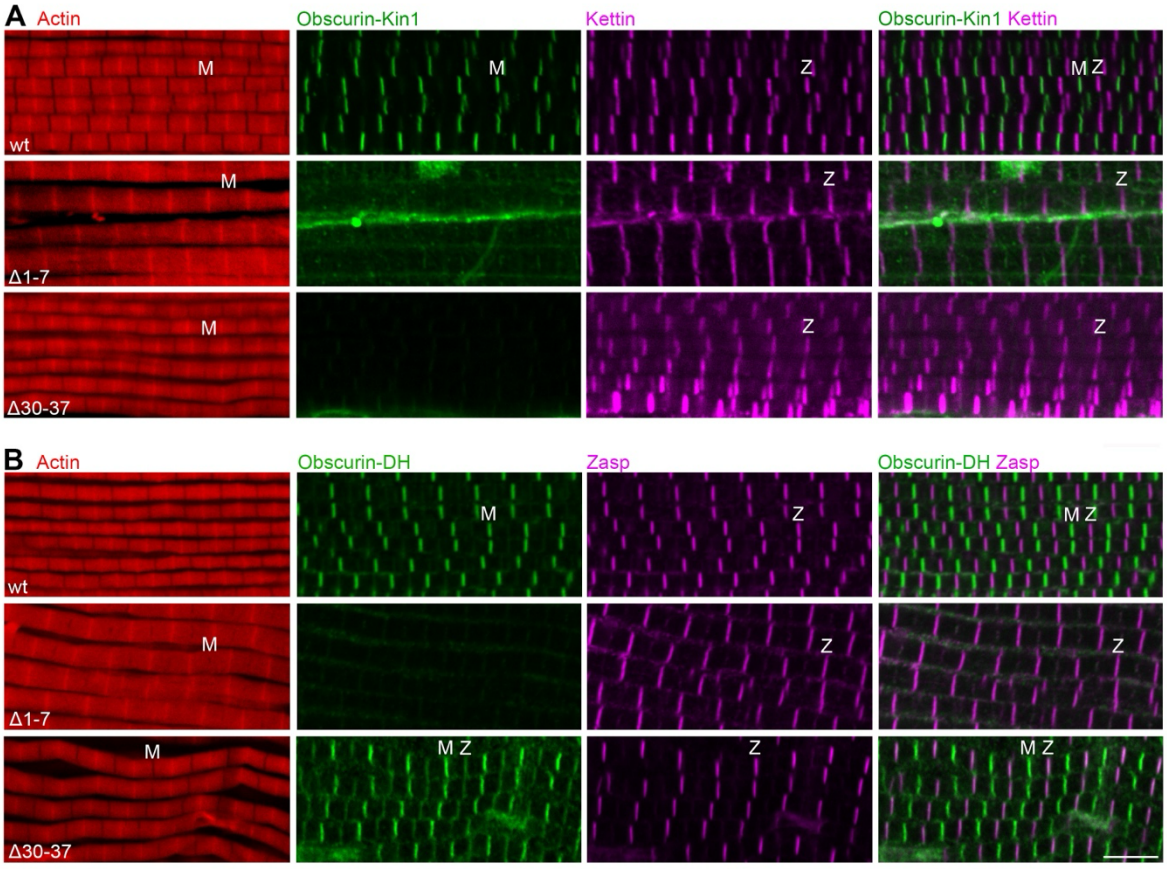

Fig. S3. Localization of disrupted obscurin isoforms in adult myofibrils. (A) Confocal microscopy images of adult IFMs of 3 d-old flies labelled with phalloidin (red, actin), anti-obscurin-Kin1 (green, M-line), and anti-Kettin (magenta, Z-disc). Kin1-containing isoforms can be weakly detected at the residual M-lines at the myofibril core in Δ1-7. (B) Adult IFMs labelled with phalloidin (red, actin), anti-obscurin-DH (green, M-line), and anti-Zasp (magenta, Z-disc). Truncated DH-containing isoforms are present in Δ30-37 and localize to the distorted M-line. Slight Z-disc labeling with anti-obscurin-DH is also observed in this mutant. Whether this reflects specific localization or nonspecific staining cannot be determined. Scale bar = 5 μm.

Journal of Cell Science • Supplementary information

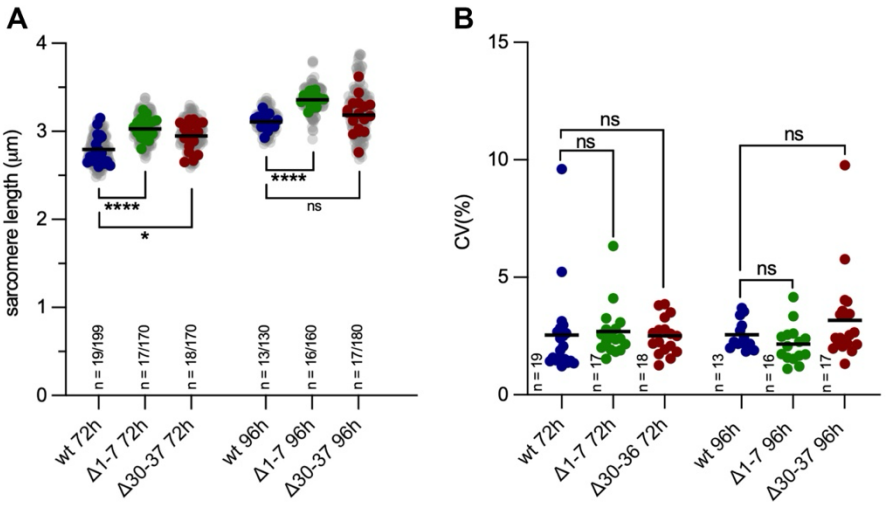

Fig. S4. Analysis of sarcomere length in pupal IFM. (A) Length measurements across genotypes at 72 h and 96 h APF. Colored dots indicate the average value for each animal, derived from 10–15 myofibrils per specimen, while grey dots represent individual measurements. Bars denote the overall mean. *n* values are shown below each genotype as *n* = number of animals/number of individual measurements. (B) Intra-animal variability in sarcomere length, shown as the coefficient of variation (CV). Statistical analysis was performed using one-way ANOVA with Dunnett's multiple comparisons test relative to wild type. Adjusted P values are indicated. ns (not significant); * $P < 0.05$; **** $P < 0.0001$.

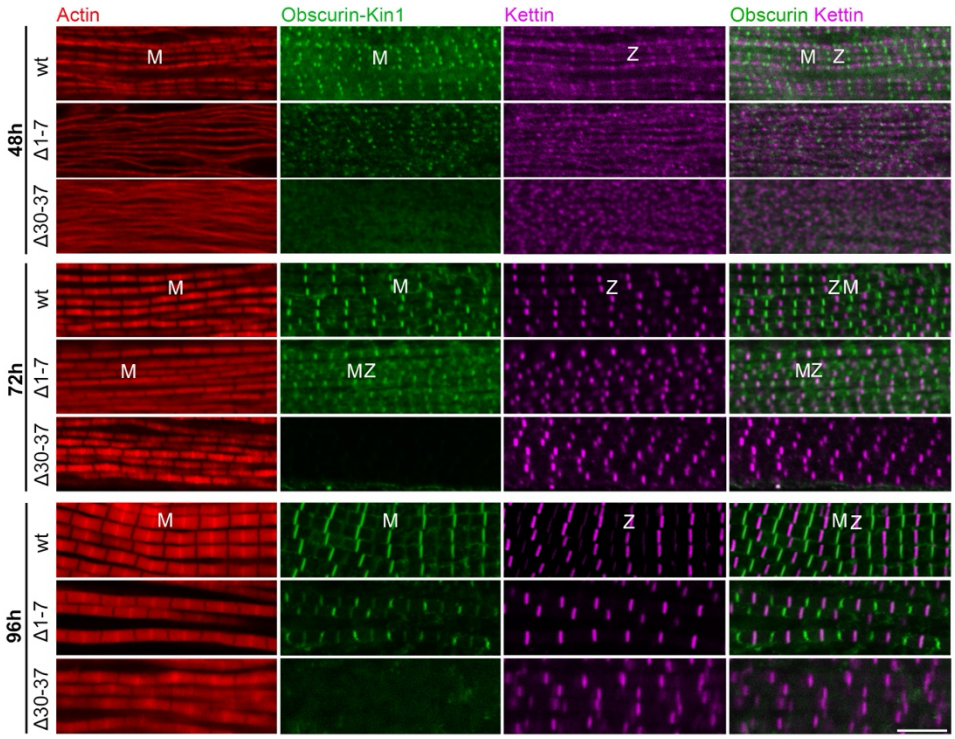

Fig. S5. Smaller kinase-containing obscurin isoforms are present in the Δ1–7 mutant during pupal IFM development. Wild-type and mutant IFM were stained with phalloidin (red, actin), anti-obscurin–Kin1 (green, M-line), and anti-Kettin (magenta, Z-disc) at 48 h, 72 h, and 96 h APF. In the Δ1–7 mutant, Kin1-containing obscurin isoforms are detected at the core of the M-line from 48 h APF onward. At this stage, the reduced myofibrillar organization correlates with a less regular M-line localization. At 72 h APF, Kin1-containing isoforms additionally localize to the Z-disc. By 96 h APF, obscurin–Kin1 localization is predominantly confined to the M-line. In the Δ30–37 mutant, no Kin1 signal is detected at any stage, consistent with deletion of the antibody epitope. Scale bar = 5 μm.

Journal of Cell Science • Supplementary information

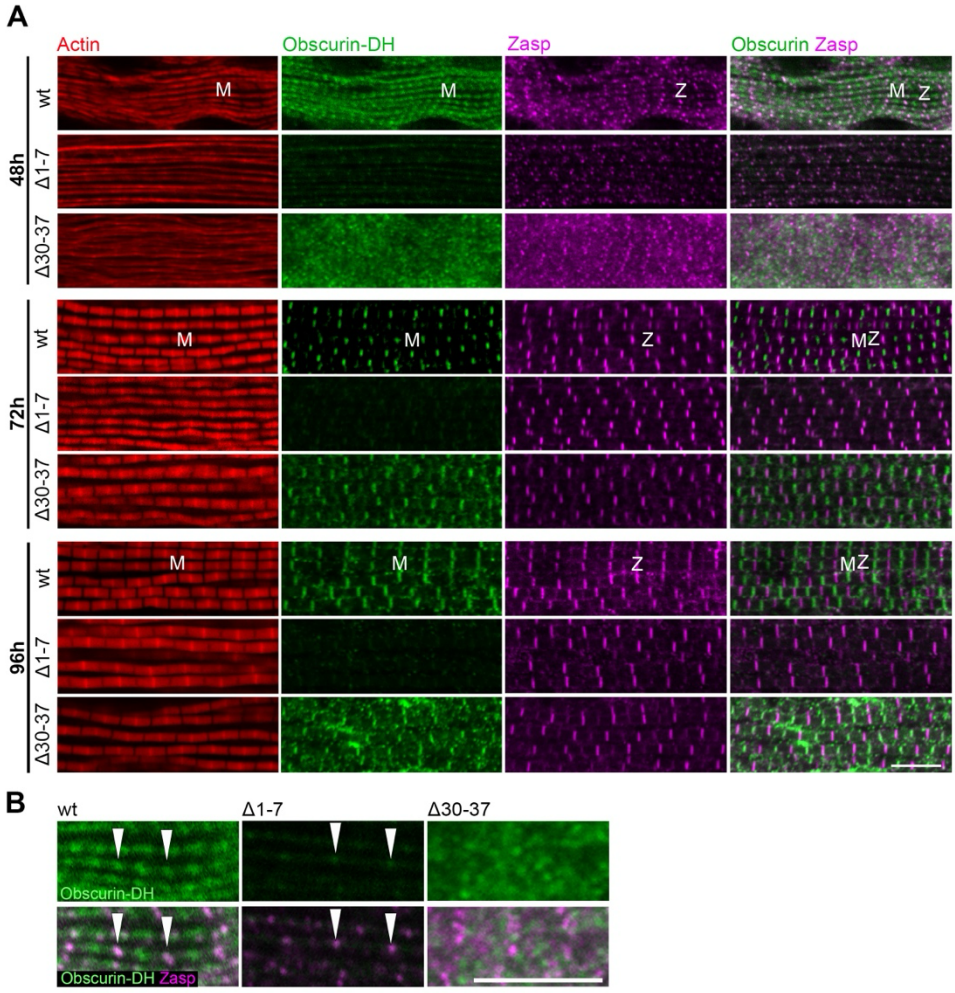

Fig. S6. Localization of DH-containing obscurin isoforms during pupal development. (A) Wild type and mutant IFM were stained with phalloidin (red, actin), anti-obscurin-DH (green, M-line), and anti-Zasp (magenta, Z-disc) at 48 h, 72 h, and 96 h APF. In wild type IFMs at 48 h APF, DH-containing obscurin isoforms are detected at both the M-line and the Z-disc, providing evidence for a transient Z-disc localization of obscurin during early myofibrillogenesis. By 72 h APF, DH-containing isoforms are predominantly localized to the M-line. This pattern is maintained at 96 h APF. In the Δ1–7 mutant, which lacks the DH antibody epitope, only weak Z-disc–associated signal is detected at 48 and 72 h APF, consistent with minor nonspecific antibody staining. In the Δ30–37 mutant, obscurin-DH signal is initially diffuse at 48 h APF, lacking a defined sarcomeric localization. By 72 h APF, truncated DH-containing isoforms localize to the M-line in a slightly disrupted pattern, which persists at 96 h APF. (B) Higher-magnification images of 48 h IFM showing possible Z-disc localization of DH-containing obscurin isoforms (white arrowheads) in wild-type muscle compared with the Δ1–7 mutant, which lacks the DH epitope. Scale bar = 5 μm.

Journal of Cell Science • Supplementary information

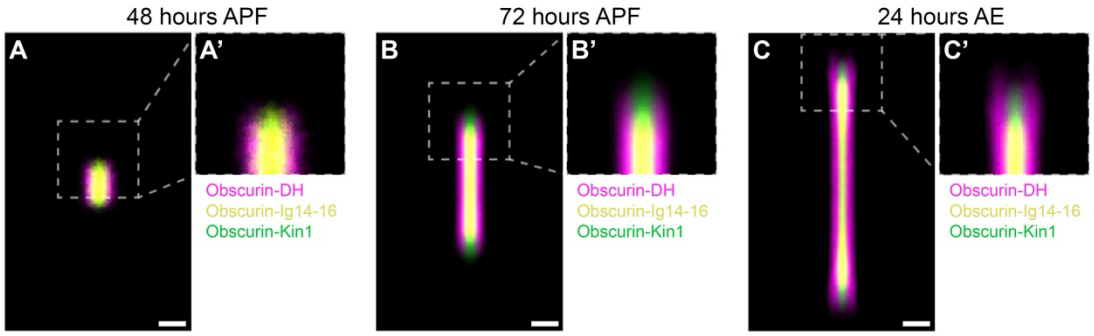

Fig. S7. Averaged pseudo-multicolor dSTORM reconstructions of IFM myofibrils during myofibrillogenesis. Shown is the arrangement of obscurin Ig14–16, obscurin Kin1, and obscurin DH epitopes at 48 h APF, 72 h APF, and 24 h AE. Panels (A–C) illustrate the progressive increase in myofibril diameter during development, while the insets (A',B',C') highlight the myofibril periphery, where the Ig14–16 epitope is consistently absent from the extreme edge, whereas the Kin1 and DH epitopes are present. Scale bar = 200 nm.

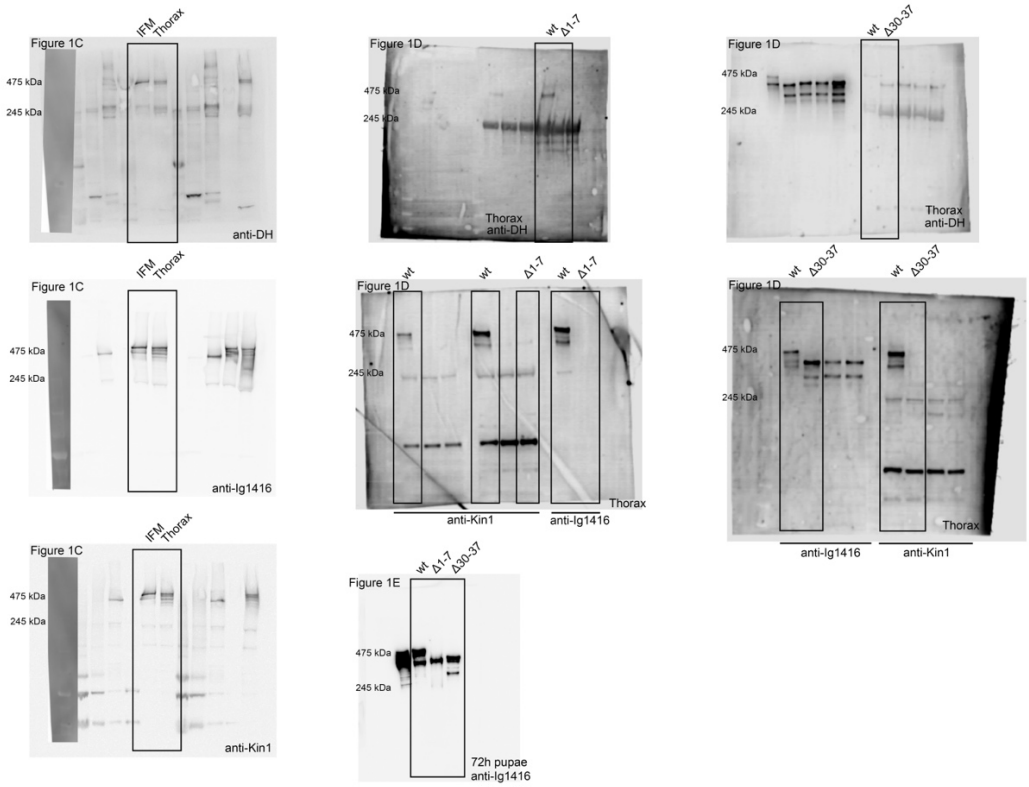

Fig. S8. Source Data. All uncropped Western Blots are shown, with the lanes used in Figure 1 framed.

Journal of Cell Science • Supplementary information